from that bound to the functional ASEs, and it does not function as an age-related regulatory element [27]. Furthermore, two other ASE-like known Ets consensus elements, one in the first intron (GAGGATG) and the other in the last exon (CAGGATG), bind an identical nuclear protein, but again different from the protein which binds to the functional ASEs (G/CAGGAAG). These elements also do not function for age-related gene regulation. Together, these results indicate that specific single base differences in the motif G/CAGGAA/TG/A facilitate strictly selective binding of specific Ets family nuclear proteins, thus conferring distinctly different functions. As we tested in transgenic mice, hFIX ASE could functionally substitute hPC ASE in the regulation of hPC gene expression [27]. ASE functions through binding a unique, probably Ets, family transcription factor. Its identification and characterization studies are in progress.

The hPC gene does not have any AIE-like element. However, as demonstrated by animal testing with minigene −1462hPCm1/AIE, which contains a unit of hFIX AIE, the age-stable expression pattern of hPC was dramatically changed to an age-related increase pattern, similar to that of the hFIX gene [27]. The mechanism of action of AIE remains to be established. These findings, together with other observations, support the functional universality of ASE and AIE. Animal testing of the mouse gene counterpart of the hFIX AIE in combination with hPC ASE has proved its functionality. Thus, the molecular mechanisms involving ASE and AIE function across different species, at least within human and mouse physiologies.

Through differential or combined usages of ASE and AIE most, if not all, anti- or procoagulation factor genes may achieve age-related increase or stable gene expression patterns, respectively. Our observations that there are no significant differences in the rate of protein clearance from the circulation between young and old animals, either for hFIX or hPC, support this further [26,27]. Together, these observations explain how the age-related increase pattern of the overall blood coagulation activity is generated (Fig. 5). Nature may also use the mechanisms for many other genes involved in different physiological systems for their age-related regulation. Further studies in this regard are under way.

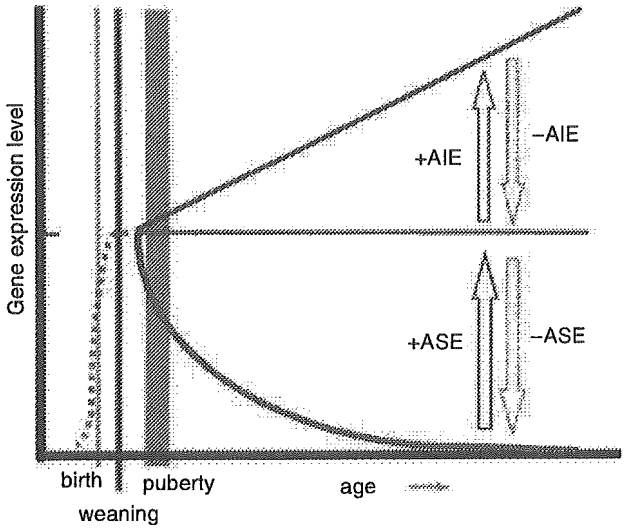

Fig. 5. The first molecular mechanisms of age-related regulation of genes and the principle of ADT. Functions of ASE and AIE in age-related regulation of gene expression are shown schematically. ASE is required for stabilization of gene expression at the prepubertal level, while AIE in the presence of ASE is responsible for age-related increase in gene expression. AIE requires the presence of ASE for its optimal function. If AIE, but not ASE is removed (shown as –AIE), gene expression is stabilized and in addition, if ASE is also removed (shown as –ASE), gene expression becomes unstable in relation to the age-axis. These findings support the possibility for developing age-related gene manipulation technology (ADT).

Development of age-dimension technology

New knowledge of the molecular mechanisms of age-dimension homeostasis allows us to develop a new research field, age-dimension technology (ADT). Through manipulating ASE and AIE activities, for instance, by using new drugs designed to affect the functions of ASE and/or AIE, we may be able to modify gene expression along the age axis, thus leading to the development of novel preventive and therapeutic methods for age-related diseases. Some anticipated examples of ADT applications may include the following.

One of the challenging difficulties facing the current efforts in developing effective and safe gene therapy approaches is how to secure a long-term effective gene expression *in vivo* after the initial single procedure of gene delivery without repeating it. ADT, which allows manipulation of expression vectors with ASE and AIE, has the great potential to make it feasible, generating optimal gene delivery systems.

Another example of ADT application is described as follows. During our studies involving a large number of transgenic mice, we found that animals overexpressing hFIX at higher than certain levels (approximately 1500 ng mL^{-1} serum) die at young ages as early as 3–5 months, while control animals or animals expressing hFIX at low levels (at less than 200 ng mL^{-1} levels) live a normal life span as expected [39] (Fig. 6). In these transgenic animals, hFIX produced was additive to the mouse intrinsic FIX.

Analyses of animals dying at much younger ages than the expected age showed thrombi present in blood vessels of various tissues including the brain, lungs and heart. Some animals developed myocardial fibrosis in the left ventricle presumably induced by thrombotic occlusions of blood vessels, thus mimicking a type of human myocardial infarction. These findings indicated that even a relatively small elevation in the circulatory level of FIX, which occupies a position in the middle phase of the blood coagulation cascade, significantly shifts the blood coagulation–anticoagulation balance toward prothrombosis. Such a thrombotic tendency, however, may be eliminated effectively by suppressing the AIE function, for instance, by designing a drug antagonistic to AIE, while keeping the ASE function intact, ensuring the needed coagulation activity.

In summary, we have discovered the very first molecular mechanisms of age-related gene regulation, explaining the

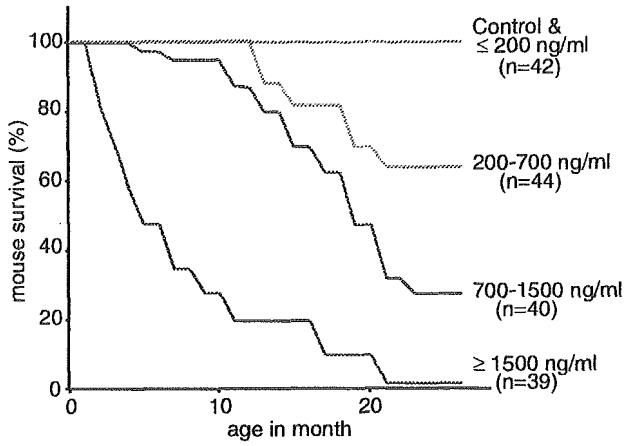

Fig. 6. Kaplan–Meier plot of transgenic mouse survival (vertical axis), level of hFIX expression and age (horizontal axis). Modified from Ameri *et al.* [39].

basic mechanisms of the age-dimension homeostasis of the blood coagulation system. This has also opened the door for discovering novel molecular mechanisms in action for age-related homeostasis of many other physiological systems.

References

1 White RH. The epidemiology of venous thromboembolism. *Circulation* 2003; **107**: 4–8.
2 Anderson FA Jr, Spencer FA. Risk factors for venous thromboembolism. *Circulation* 2003; **107**: 9–16.
3 Lusis AJ. Atherosclerosis. *Nature* 2000; **407**: 233–41.
4 Lakatta EG, Levy D. Arterial and cardiac aging: major shareholders in cardiovascular disease enterprises: part I. Aging arteries: a 'set up' for vascular disease. *Circulation* 2003; **107**: 139–46.
5 Lakatta EG, Levy D. Arterial and cardiac aging: major shareholders in cardiovascular disease enterprises: part II. The aging heart in health: links to heart disease. *Circulation* 2003; **107**: 346–54.
6 Ariesen MJ, Claus SP, Rinkel GJ, Algra A. Risk factors for intracerebral hemorrhage in the general population: a systematic review. *Stroke* 2003; **34**: 2060–5.
7 Petersen KF, Befroy D, Dufour S, Dziura J, Ariyan C, Rothman DL, DiPietro L, Cline GW, Shulman GI. Mitochondrial dysfunction in the elderly: possible role in insulin resistance. *Science* 2003; **300**: 1140–2.
8 DePinho RA. The age of cancer. *Nature* 2000; **408**: 248–54.
9 Morrison JH, Hof PR. Life and death of neurons in the aging brain. *Science* 1997; **278**: 412.
10 Bartzokis G. Age-related myelin breakdown: a developmental model of cognitive decline and Alzheimer's disease. *Neurobiol Aging* 2004; **25**: 5–18.
11 Lowe GD, Rumley A, Woodward M, Morrison CE, Philippou H, Lane DA, Tunstall-Pedoe H. Epidemiology of coagulation factors, inhibitors and activation markers: the Third Glasgow MONICA Survey. I. Illustrative reference ranges by age, sex and hormone use. *Br J Haematol* 1997; **97**: 775–84.
12 Ershler WB, Keller ET. Age-associated increased interleukin-6 gene expression, late-life diseases, and frailty. *Annu Rev Med* 2000; **51**: 245–70.
13 Linton PJ, Dorshkind K. Age-related changes in lymphocyte development and function. *Nat Immunol* 2004; **5**: 133–9.
14 Dahlback B. Blood coagulation. *Lancet* 2000; **355**: 1627–32.
15 Andrew M, Vegh P, Johnston M, Bowker J, Ofosu F, Mitchell L. Maturation of the hemostatic system during childhood. *Blood* 1992; **80**: 1998–2005.
16 Mari D, Mannucci PM, Coppola R, Bottasso B, Bauer KA, Rosenberg RD. Hypercoagulability in centenarians: the paradox of successful aging. *Blood* 1995; **85**: 3144–9.
17 Conlan MG, Folsom AR, Finch A, Davis CE, Sorlie P, Marcucci G, Wu KK. Associations of factor VIII and von Willebrand factor with age, race, sex, and risk factors for atherosclerosis: the Atherosclerosis Risk in Communities (ARIC) Study. *Thromb Haemost* 1993; **70**: 380–5.
18 Balleisen L, Bailey J, Epping PH, Schulte H, van de Loo J. Epidemiological study on factor VII, factor VIII and fibrinogen in an industrial population. I. Baseline data on the relation to age, gender, body-weight, smoking, alcohol, pill-using, and menopause. *Thromb Haemost* 1985; **54**: 475–9.
19 Wilkerson WR, Sane DC. Aging and thrombosis. *Semin Thromb Hemost* 2002; **28**: 555–68.
20 Conlan MG, Folsom AR, Finch A, Davis CE, Marcucci G, Sorlie P, Wu KK. Antithrombin III: associations with age, race, sex and cardiovascular disease risk factors. The Atherosclerosis Risk in Communities (ARIC) Study Investigators. *Thromb Haemost* 1994; **72**: 551–6.
21 Bauer KA, Weiss LM, Sparrow D, Vokonas PS, Rosenberg RD. Aging-associated changes in indices of thrombin generation and protein C activation in humans. Normative Aging Study. *J Clin Invest* 1987; **80**: 1527–34.
22 Takada Y, Takada A. Plasma levels of t-PA free PAI-1 and a complex of t-PA with PAI-1 in human males and females at various ages. *Thromb Res* 1989; **55**: 601–9.
23 Ofosu FA, Craven S, Dewar L, Anvari N, Andrew M, Blajchman MA. Age-related changes in factor VII proteolysis *in vivo*. *Br J Haematol* 1996; **94**: 407–12.
24 Hirsh J, Fuster V, Ansell J, Halperin JL. American Heart Association/American College of Cardiology Foundation guide to warfarin therapy. *Circulation* 2003; **107**: 1692–711.
25 Sweeney JD, Hoernig LA. Age-dependent effect on the level of factor IX. *Am J Clin Pathol* 1993; **99**: 687–8.
26 Kurachi S, Deyashiki Y, Takeshita J, Kurachi K. Genetic mechanisms of age regulation of human blood coagulation factor IX. *Science* 1999; **285**: 739–43.
27 Zhang K, Kurachi S, Kurachi K. Genetic mechanisms of age regulation of protein C and blood coagulation. *J Biol Chem* 2002; **277**: 4532–40.
28 Yoshitake S, Schach BG, Foster DC, Davie EW, Kurachi K. Nucleotide sequence of the gene for human factor IX (antihemophilic factor B). *Biochemistry* 1985; **24**: 3736–50.
29 Miao CH, Ho WT, Greenberg DL, Davie EW. Transcriptional regulation of the gene coding for human protein C. *J Biol Chem* 1996; **271**: 9587–94.
30 Foster DC, Yoshitake S, Davie EW. The nucleotide sequence of the gene for human protein C. *Proc Natl Acad Sci USA* 1985; **82**: 4673–7.
31 Kurachi S, Hitomi Y, Furukawa M, Kurachi K. Role of intron I in expression of the human factor IX gene. *J Biol Chem* 1995; **270**: 5276–81.
32 Xin J-H, Cowie A, Lachance P, Hassell JA. Molecular cloning and characterization of PEA3, a new member of the Ets oncogene family that is differentially expressed in mouse embryonic cells. *Genes Dev* 1992; **6**: 481–96.
33 Chotteau-Lelievre A, Desbiens X, Pelczar H, Defossez P-A, Launoit Y. Differential expression patterns of the PEA3 group transcription factors through murine embryonic development. *Oncogene* 1997; **15**: 937–52.
34 Yao S-N, DeSilva AH, Kurachi S, Samuelson LC, Kurachi K. Characterization of a mouse factor IX cDNA and developmental

regulation of the factor IX gene expression in liver. *Thromb Haemost* 1991; **65**: 52–8.

35 Kurachi S, Hitomi E, Kurachi K. Age and sex dependent regulation of the factor IX gene in mice. *Thromb Haemost* 1996; **76**: 965–9.

36 Wu S-M, Stafford DW, Ware J. Deduced amino acid sequence of mouse blood-coagulation factor IX. *Gene* 1990; **86**: 275–8.

37 Salier J-P, Hirosawa S, Kurachi K. Functional characterization of the 5′-regulatory region of human factor IX gene. *J Biol Chem* 1990; **265**: 7062–8.

38 Hsu W, Kawamura S, Fountaine J-M, Kurachi K, Kurachi S. Organization and significance of LINE-1-derived sequences in the 5′ flanking region of the factor IX gene. *Thromb Haemost* 1999; **82**: 1782–3.

39 Ameri A, Kurachi S, Sueishi K, Kuwahara M, Kurachi K. Myocardial fibrosis in mice with overexpression of human blood coagulation factor IX. *Blood* 2003; **101**: 1871–3.

Effect of Hydrodynamics-Based Gene Delivery of Plasmid DNA Encoding Interleukin-1 Receptor Antagonist-Ig for Treatment of Rat Autoimmune Myocarditis

Possible Mechanism for Lymphocytes and Noncardiac Cells

Hui Liu, MD; Haruo Hanawa, MD; Tsuyoshi Yoshida, MD; Raafat Elnaggar, MD; Manabu Hayashi, MD; Ritsuo Watanabe, MD; Ken Toba, MD; Kaori Yoshida, BS; He Chang, MD; Yuji Okura, MD; Kiminori Kato, MD; Makoto Kodama, MD; Hiroki Maruyama, MD; Junichi Miyazaki, MD; Mikio Nakazawa, PhD; Yoshifusa Aizawa, MD

Background—Interleukin-1 (IL-1) is a powerful and important cytokine in myocarditis. The purpose of this study was to evaluate the effect and possible mechanism of hydrodynamics-based delivery of the IL-1 receptor antagonist (IL-1RA)-immunoglobulin (Ig) gene for treatment of rat experimental autoimmune myocarditis (EAM).

Methods and Results—On the day after immunization, rats were transfected with either pCAGGS encoding IL-1RA-Ig or pCAGGS encoding Ig alone. On day 17, IL-1RA-Ig gene therapy was effective in controlling EAM, as monitored by a decreased ratio of heart weight to body weight, reduced myocarditis areas, reduced gene expression of atrial natriuretic peptide in hearts, and improved cardiac function in echocardiographic and hemodynamic parameters. Examination of the expression of IL-1–related genes in purified cells from EAM hearts suggested that ectopic IL-1RA-Ig–acting target cells were $\alpha\beta$T cells and noncardiomyocytic noninflammatory cells such as fibroblasts, smooth muscle cells, and endothelial cells. Therefore, we examined the effect of serum containing IL-1RA-Ig on the expression of immune-relevant genes within noncardiomyocytic cells cultured from EAM hearts or concanavalin A–stimulated lymphocytes derived from lymph nodes in EAM-affected rats. The expression of immunologic molecules (prostaglandin E synthase, cyclooxygenase-2, and IL-1β) in cultivated noncardiomyocytic cells and Th1 cytokines (IL-2 and IFN-γ) in lymphocytes was significantly decreased by the serum containing IL-1RA-Ig.

Conclusions—EAM was suppressed by hydrodynamics-based delivery of plasmid DNA encoding IL-1RA-Ig. In addition, IL-1RA-Ig suppressed gene expression of prostaglandin synthases and IL-1 in noncardiomyocytic cells and Th1 cytokines in lymphocytes. (***Circulation.*** **2005;111:1593-1600.)**

Key Words: cardiomyopathy, dilated ■ cytokines ■ sialoglycoproteins ■ myocarditis ■ prostaglandins

Rat experimental autoimmune myocarditis (EAM) resembles human giant cell myocarditis,[1] and recurrent forms lead to dilated cardiomyopathy.[2] Histopathological investigation showed that CD11b$^+$ cells (macrophages, dendritic cells, granulocytes) and CD4$^+$ T cells infiltrated the heart, which severely injured cardiomyocytes in the acute stage, followed by fibrosis in the heart.[3] Various cytokines have been found in EAM-affected hearts.[4]

Interleukin-1 (IL-1), formerly known as lymphocyte activating factor, is an important inflammatory cytokine produced by monocytes, macrophages, dendritic cells, B cells, or NK cells.[5,6] There are 2 structurally distinct forms of IL-1, IL-1α and IL-1β, which are both potent stimulators of target cells.[5,7] IL1-β, which has a signal peptide and is excreted from cells, is important for regional inflammation.[8] The IL-1 receptor (IL-1R) is divided into 2 structurally distinct forms, namely IL-1 receptor 1 (IL-1RI) and II (IL-1RII). IL-1RI expressed on T cells and fibroblasts among other cell types,[9] when bound to IL-1, forms heterocomplexes with IL-1 receptor accessory protein (IL-1Racp) and thereby transduces intracellular signals.[10] However, IL-1RII consisting of IL-1 binding portion, a single transmembrane region, and a shorter cytoplasmic domain cannot transduce signals and acts as a decoy target.[11] On the other hand, there are 2 structurally distinct forms of IL-1 receptor antagonist (IL-1RA) made by alternative splicing: secreted IL-1RA (sIL-1RA) and intracel-

Received May 26, 2004; revision received November 5, 2004; accepted November 10, 2004.

From the Divisions of Cardiology (H.L., H.H., T.Y., R.E., M.H., R.W., K.T., K.Y., H.C., Y.O., K.K., M.K., Y.A.) and Clinical Nephrology and Rheumatology (H.M.), Niigata University Graduate School of Medical and Dental Sciences, and Department of Medical Technology, School of Health Sciences, Faculty of Medicine (M.N.), Niigata University, Niigata, and Division of Stem Cell Regulation Research, Osaka University Medical School (J.M.), Suita, Japan.

Correspondence to H. Hanawa, Division of Cardiology, Niigata University Graduate School of Medical and Dental Sciences, 1-757 Asahimachi-dori, Niigata 951-8120, Japan. E-mail hanawa@med.niigata-u.ac.jp

Circulation **is available at http://www.circulationaha.org** **DOI: 10.1161/01.CIR.0000160348.75918.CA**

lular IL-1RA (icIL-1RA).[12] IL-1RA functions as an antagonist by competitively binding to IL-1RI.[13,14] IL-1RA cannot transduce intracellular signals because it is unable to bind to IL-1Racp.[12,15] IL-1RA–based therapies are being evaluated for a variety of diseases.[16–18]

The purpose of the present study was to investigate whether IL-1RA transduction ameliorated EAM and by what mechanisms this therapy occurred. Hydrodynamics-based gene transfer via the rapid tail vein injection of a large volume is more efficient than delivery by intramuscular injection with electroporation.[19,20] This method can retrogradely deliver plasmid DNA predominantly into hepatocytes via hepatic vein. Moreover, chimeras with immunoglobulin (Ig) facilitate elevated concentration levels.[21] In this study, we examined the efficacy of hydrodynamics-based delivery of plasmid DNA encoding an IL-1RA-Ig chimera.

Methods

Animals

Seven-week-old male Lewis rats were purchased from Charles-River Laboratories, Japan (Atsugi, Kanagawa, Japan) and were maintained in our animal facilities. Throughout the studies, all the animals were treated in accordance with the guidelines for animal experiments as laid out by our institute.

Induction of EAM

Cardiac myosin was prepared from the ventricular muscle of porcine hearts as previously described.[1] To produce EAM, each rat was immunized on day 0 with 0.2 mL emulsion containing cardiac myosin with an equal volume of complete Freund's adjuvant by a single subcutaneous injection in both footpads.

In Vivo Treatment of EAM With Plasmid DNA Encoding IL-1RA-Ig Gene

Construction of Plasmid DNA for Gene Transfer

We first constructed the plasmid vector pCAGGS-Ig-glucagon (Glu)-tag, containing *Swa*I and *Not*I restriction sites, via polymerase chain reaction (PCR) amplification. For this purpose, initial PCR products were generated from rat spleen cDNA using KOD Plus DNA polymerase (Toyobo) and the following primers: 5′-gaGAATTCATTTAAATgagaGCGGCCGCgtgcccagaaactgtg-3′ (contains both *Swa*I and *Not*I restriction sites) and 5′-tcaaccactgcacaaaatcttgggctttacccggagagtgggagagact-3′. The final PCR product inserts were then amplified from the diluted products of the first PCR reaction with the following primers: 5′-gaGAATTCATTTAAATgagaGCGGCCGCgtgcccagaaactgtg-3′ (as before) and 5′-gagagagaGAATTCtcaggtattcatcaaccac-tgcacaaaattcttgggc-3′. Finalized PCR products were inserted into the pCAGGS vector using *Eco*RI sites. *Escherichia coli* JM109 competent cells were then transformed, and recombinant plasmids were isolated by use of a Quantum Prep Plasmid Maxiprep kit (Bio-Rad Laboratories). To construct the control plasmid, pCAGGS-rat signal peptide (SP)-Ig-Glu-tag, the SP region of secretory leukocyte protease inhibitor, was amplified from EAM heart cDNA with the primers 5′-gaGAATTCATTTAAATgaagtccagcggcctcttcccc-3′ and 5′-gcagcatcGCGGCCGCtccttccacactccagggtgccag-3′, followed by insertion into pCAGGS-Ig-Glu-tag using *Swa*I and *Not*I sites. To construct the pCAGGS-mouse IL-1RA-Ig-Glu-tag, mouse IL-1RA was amplified from mouse splenocyte cDNA using the primers 5′-gagaattcATTTAAATggaaatctgctggggaccctac-3′ and 5′-gcagcatc GCGGCCGCttggtcttcctggaagtagaact-3′, followed by insertion into pCAGGS-Ig-Glu-tag using *Swa*I and *Not*I sites. Recombinant plasmids were isolated as described above.

Plasmid DNA Injection Techniques

Nineteen rats were divided into 2 groups, the pCAGGS-IL-1RA-Ig group (IL-1RA-Ig group; n=10) and the pCAGGS-SP-Ig group (SP-Ig group; n=9). Rats were injected with 800 μg pCAGGS-mouse IL-1RA-Ig-Glu-tag or pCAGGS-SP-Ig-Glu-tag via the tail vein within 15 seconds (receiving ≈80 mL/kg body weight) on day 1.[19]

Plasmid Chimeric Glucagons-Tag Protein Measurement

Blood samples were taken on days 2, 5, 8, 12, and 17. Glucagon concentrations were measured with a glucagons radioimmunoassay kit (Daiichi Radioisotope Laboratories).[22] Chimeric protein concentrations in blood were calculated with Glu-tag.[23] To observe the relationship of them and gene expression in liver, the livers were harvested on days 2, 5, 8, 12, and 17 after injection of pCAGGS-IL-1RA-Ig-Glu-tag into normal rats (n=4, respectively), and transgene expressions were examined by real-time reverse-transcriptase (RT) PCR using the following primers: 5′-tctgactgaccgcgttactccca-3′ (726 to 748 bases in pCAGGS) and 5′-atcagtgatgttaacttcctccag-3′ (316 to 339 bases in mouse sIL-1RA).

Evaluation of Echocardiography and Hemodynamic Parameters

On day 17, echocardiography was performed with a 7.5-MHz probe (SSD-630, Aloka ECHO camera). Left ventricular (LV) internal diameter in end diastole and end systole, interventricular septal thickness, LV posterior wall thickness, pericardial effusion (PE) under LV posterior wall thickness, and LV fractional shortening were calculated from M-mode echocardiograms over 3 consecutive cardiac cycles.

The hemodynamic parameters were measured after echocardiography. Mean arterial pressure was recorded through a catheter introduced into the right femoral artery. Central venous pressure (was recorded through a catheter introduced into the confluence of the vena cava with the right jugular vein. A catheter-tip transducer was inserted into the left ventricle from the right carotid artery to measure the peak left ventricular pressure and left ventricular end-diastolic pressure. The rates of intraventricular pressure rise and decline (±dP/dt) were measured with a differential amplifier. Heart rate was calculated from ECGs. All hemodynamic parameters were recorded on a thermostylus recorder after a stabilizing period of 10 minutes.

Evaluation of Histopathology

Heart and body weights were measured, and the ratio of heart weight to body weight (g/g) was calculated. Several transverse sections were cut from the midventricle slice and stained with Azan-Mallory. The myocarditis area of each specimen was determined with a color image analyzer (Mac SCOPE version 2.6, Mitani Corp).

Measurement of Atrial Natriuretic Peptide mRNA Levels

To measure mRNA levels of atrial natriuretic peptide (ANP), a heart failure marker, total RNA was isolated from the apical one third of the heart on day 17. The absolute copy number of ANP mRNA was measured by quantitative real-time RT-PCR.

Gene Expression of IL-1 Family in EAM Hearts

To evaluate crosstalk between members of the IL-1 family, the mRNA levels of IL-1α, IL-1β, IL-1RI, IL-1RII, IL-1Racp, sIL-1RA, or total IL-1RA (sIL-1RA+icIL-1RA) in both isolated and purified cells from EAM hearts were measured. On day 18, cardiomyocytes and the other cells in the hearts of EAM rats were isolated after collagenase perfusion treatment for 20 minutes with a Langendorff apparatus as reported previously.[24,25] Isolated cells, while maintained in an isotonic buffer, were separated serially through stainless steel sieves into cardiomyocytes and the other cells. Because the inflammatory cells are almost $CD11b^+$ cells (macrophages/dendritic cells/granulocytes) and αβT cells,[3] the other cells without cardiomyocytes were separated into αβT cells, $CD11b^+$ cells, and noncardiomyocytic noninflammatory (NCNI) cells (mainly fibroblasts, smooth

TABLE 1. Absolute Copy Numbers of Specific Cell Marker mRNA in Cultivated Cells

	Copy Numbers of mRNA/μg of Total RNA	
	NC Cells (n=6)	Lymph Node Cells (n=6)
CD3	37 600±6300	1 490 000±215 000
Collagen type III	149 000 000±10 500 000	170 000±15 000
Calponin	23 400 000±2 110 000	ND
CD11b	11 800 000±977 000	19 000±4200
von Willebrand factor	194 000±31 000	262 000±56 000
α-Cardiac myosin	ND	ND

Results are expressed as mean±SEM.

muscle cells, and endothelial cells) by anti-PE micro beads (Miltenyi Biotec) and an MACS magnetic cell sorting system (Miltenyi Biotech) using appropriate monoclonal antibodies, namely PE-conjugated TCRα/β (R73) and CD11bc (OX-42) (Pharmingen).[26] The fractions of cardiomyocytes, αβT cells, $CD11b^+$ cells, and NCNI cells were confirmed by analysis of specific marker gene expression—α-cardiac myosin, CD3, CD11b, collagen type III, calponin, and von Willebrand factor—and even if the level of contamination was the highest, it was <10% (data not shown). Total RNA was isolated from each purified cell fraction (cardiomyocytes, n=5; αβT cells, n=5; $CD11b^+$ cells, n=5; NCNI cells, n=6). The absolute copy numbers of IL-1 family mRNA were measured by quantitative real-time RT-PCR.

Cell Culture With Serum Containing IL-1RA-Ig

NC Cells

On day 18, NC cells were isolated from the hearts of EAM rats via collagenase preparation and were cultured for 1 week on 35-mm–well dishes in 3 mL RPMI medium supplemented with 10% FCS. These cultivated NC cells were suggested to contain mainly fibroblasts, smooth muscle cells, and $CD11b^+$ cells, as determined by gene expression analysis (Table 1). After reaching confluence, NC cells were stimulated by addition of 10 ng/mL IL-1α (Pepro Tech) and 100 μL IL-1RA-Ig-Glu-tag–containing serum (30 nmol/L) or the same amount of Ig-Glu tag–containing serum (IL-1RA-Ig+IL-1α group, n=6; SP-Ig+IL-1α group, n=6; no serum and no IL-1α group, n=6). After culture for 24 hours at 37°C, NC cells were collected and total RNA was isolated. The absolute copy numbers of γ-actin, prostaglandin E synthase (PGES), cyclooxygenase-2 (Cox-2), and IL-1β mRNA were measured by quantitative real-time RT-PCR.

Lymphocytes

Lymphocytes isolated from popliteal lymph nodes of EAM rat were prepared in 3 mL RPMI medium supplemented with 10% FCS in 35-mm–well dishes. These cells were thought to be mainly lymphocytes, as indicated by expression of the CD3 gene (Table 1). Because transfer of concanavalin A (Con-A)–stimulated lymphocytes from EAM popliteal lymph nodes could induce EAM[27] and Con-A–stimulated lymphocytes can express the IL-1RI gene (data not shown), we stimulated these cells with 10 μg/mL Con-A (Sigma) and 10 ng/mL IL-1α at 6×10^6 cells per dish. One hundred microliters of IL-1RA-Ig-Glu-tag–containing serum (30 nmol/L) or the same amount of Ig-Glu-tag–containing serum was added (IL-1RA-Ig+Con-A+IL-1α, n=6; SP-Ig+Con-A+IL-1α, n=6; no serum, no Con-A, and no IL-1α, n=6). After culture for 24 hours at 37°C, these cells were collected and total RNA was isolated. The absolute copy numbers of γ-actin, IL-2, and IFN-γ mRNA were measured by quantitative real-time RT-PCR.

Quantitative Real-Time RT-PCR Analysis

Total RNA was extracted by use of Trizol (Invitrogen). cDNA was synthesized from 2 to 5 μg total RNA with random primers and murine Moloney leukemia virus RT. To create the plasmids used for the standard, the cDNAs for ANP, specific cell markers, IL-1 family proteins, and immunologic molecules were amplified from an EAM heart–derived cDNA library with the primers indicated in Table 2. PCR-amplified cDNA inserts were directly inserted into the pGEM-T easy vector, and the recombinant plasmids were isolated, after transformation into *E coli* JM109 competent cells, with the MagExtractor plasmid kit (Toyobo). Diluted plasmid and cDNA were amplified via real-time RT-PCR with a Lightcycler, together

TABLE 2. List of Primers for Quantitative RT-PCR

	Sense Primer	Antisense Primer
ANP	5′-atggatttcaagaacctgctagac-3′	5′-gctccaatcctgtcaatcctac-3′
α-Cardiac myosin	5′-acaaggttaaaaacctgacagagg-3′	5′-tactgttctgctgactgatgtcaa-3′
CD3	5′-gatcccaaactctgctatatgcta-3′	5′-ctttcatgccaatctcactgtag-3′
CD11b	5′-gggatccgtaaagtagtgagaa-3′	5′-aaaggagctggtacttcctgtct-3′
Collagen type III	5′-cgcaattgcagagacctgaa-3′	5′-acagtcatgggactggcatttat-3′
von Willebrand factor	5′-agaggctacacatctctcagaagc-3′	5′-gaccttcttcttcttgaaaccttg-3′
Calponin	5′-aacataggaaatttcatcaaagcc-3′	5′-gtagactgatagttgcctgatcca-3′
IL-1α	5′-aagttcctgacttgtttgaagacc-3′	5′-gtcatcttcagtaaagggctgatt-3′
IL-1β	5′-gctagtgtgtgatgttcccattag-3′	5′-cttttccatcttcttctttgggta-3′
IL-1RI	5′-ataaactgatggtgatgaatgtgg-3′	5′-tgagagtgaactttcttttggctg-3′
IL-1RII	5′-gttatgacatttacctacgagggc-3′	5′-ctttgtgactggatcaaaaatcag-3′
IL-1Racp	5′-ctggacttaccctgatctggtacg-3′	5′-acacgtgatattgtgaataccctg-3′
sIL-1RA	5′-tctctctccttctcatccttctgt-3′	5′-atcagtgatgttaacctcctccag-3′
Total IL-1RA	5′-agaagaaaagatagacatggtgcc-3′	5′-actttgtgactgtacagggctctt-3′
IL-2	5′-ctgagagggatcgataattacaaga-3′	5′-attggcactcaaatttgttttcag-3′
IFN-γ	5′-atctggaggaactggcaaaaggacg-3′	5′-ccttaggctagattctggtgacagc-3′
PGES	5′-gtgatggagaacagccaggt-3′	5′-gaggaccacgaggaaatgtatc-3′
Cox-2	5′-tgtgatattctcaaacaggagcat-3′	5′-aaggaggatggagttgttgtagag-3′
γ-Actin	5′-agccttccttcctgggcatggagt-3′	5′-tggaggggcctgactcgtcatact-3′

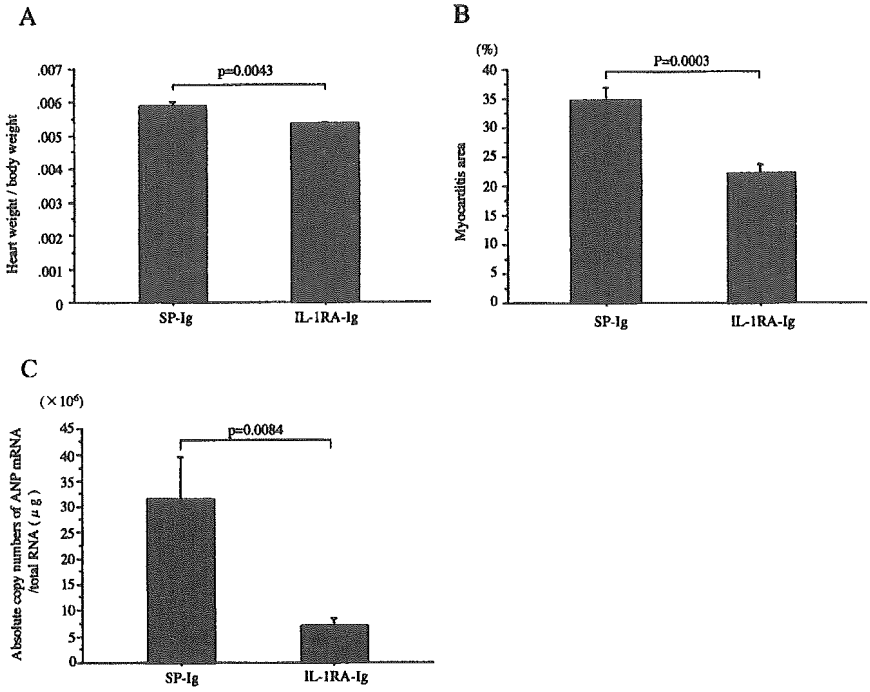

Figure 1. A, Ratio of heart weight to body weight. B, Myocarditis area in EAM heart. Area was calculated by color image analyzer using specimens stained with Azan-Mallory. C, Absolute copy number of ANP mRNA in EAM hearts. Error bars represent SEM. Statistical assessment was performed by unpaired Student *t* test. SP-Ig indicates rats that were injected with pCAGGS-rat SP-Ig-Glu-tag; IL-1RA-Ig, rats injected with pCAGGS-mouse IL-1RA-Ig-Glu-tag.

with the same primer pair used for making the plasmid and a LightCycler-FastStart DNA Master SYBR Green I kit (Roche). After an initial denaturation step of 10 minutes at 95°C, a 3-step cycling procedure (denaturation at 95°C for 10 seconds, annealing at 62°C for 10 seconds, and extension at 72°C for 13 seconds) was used for 40 cycles. The absolute copy numbers of particular transcripts were calculated by LightCycler software using a standard curve approach.[4] cDNA from cultivated cells was then subjected to quantitative RT-PCR analysis, with the level of γ-actin mRNA acting as an internal control.

Statistical Analysis

Statistical assessment was performed by unpaired Student *t* test or 1-way ANOVA and Bonferroni multiple comparison test. The differences were considered significant at $P<0.05$. Ratio of heart weight to body weight, myocarditis area, echocardiography and hemodynamic parameters, data obtained from quantitative RT-PCR, and concentration of IL-1RA-Ig-Glu-tag and Ig-Glu-tag were expressed as mean±SEM.

Results

Effect of In Vivo Treatment With Plasmid DNA Encoding IL-1RA-Ig Gene

The heart to body weight ratios in the IL-1RA-Ig group were significantly lower than those of the SP-Ig group (mean±SEM, 0.53±0.03% versus 0.59±0.05%; $P=0.0043$) (Figure 1A). The inflammatory area in the IL-1RA-Ig group was significantly smaller than that observed in the SP-Ig group (22.3±4.8% versus 34.6±6.8%, $P=0.0003$) (Figure 1B). Expression of ANP mRNA (a heart failure marker) was significantly lower in heart tissues of the IL-1RA-Ig group than those of controls (7.13×10^6±3.62×10^6 versus 31.6×10^6±24.2×10^6 copy/total RNA μg; $P=0.0084$) (Figure 1C).

Echocardiograph and Hemodynamic Parameters

As shown in Table 3, the LV fractional shortening and the absolute value of +dP/dt or −dP/dt in IL-1RA-Ig group were significantly larger than in SP-Ig group. LV end-systolic diameter, LV posterior wall thickness, PE, LV end-diastolic pressure, and central venous pressure were significantly smaller in the IL-1RA-Ig group than in SP-Ig group.

Time Course of IL-1RA-Ig-Glu-Tag Protein Levels

Plasma IL-1RA-Ig-Glu-tag protein levels in the IL-1RA-Ig group were found to increase, peaking at 23.21±8.52 nmol/L (mean±SEM) on day 2, and gradually decrease to 5.56±2.70 nmol/L on day 5, 1.64±0.63 nmol/L on day 8, 0.85±0.45 nmol/L on day 12, and 0.22±0.07 nmol/L on day 17. The plasma Ig-Glu-tag protein levels in the SP-Ig group were seen

TABLE 3. Echocardiographic and Hemodynamic Parameters

	IL-1RA-Ig (n=7)	SP-Ig (n=6)	*P*
LVEDd, mm	5.41±0.05	5.48±0.29	0.81
LVESd, mm	3.01±0.17	3.81±0.24	0.018
IVS, mm	1.84±0.05	1.96±0.12	0.33
LVPW, mm	1.89±0.17	2.24±0.27	0.012
PE, mm	1.71±0.47	3.67±0.49	0.016
LVFS, %	44.4±2.9	30.4±2.4	0.0039
HR, bpm	354.9±14.3	381.5±19.8	0.29
CVP, mm Hg	1.73±0.26	3.93±0.55	0.0029
AP, mm Hg	78.4±2.52	72.6±1.72	0.094
LVP, mm Hg	91.1±3.53	85.9±2.08	0.244
EDP, mm Hg	11.7±1.3	18.4±2.24	0.0218
+dP/dt, mm Hg/s	4459±243	3636±178	0.0226
−dP/dt, mm Hg/s	−5547±352	−4129±202	0.0067

LVEDd indicates LV end-diastolic internal diameter; LVESd, LV end-systolic internal diameter; IVS, interventricular septal thickness; LVPW, LV posterior wall thickness; LVFS, LV fractional shortening; HR, heart rate; CVP, central venous pressure; AP, mean blood pressure; LVP, peak LV pressure; EDP, LV end-diastolic pressure; +dP/dt, maximum dP/dt; and −dP/dt, minimum dP/dt.
Result are expressed as mean±SEM.

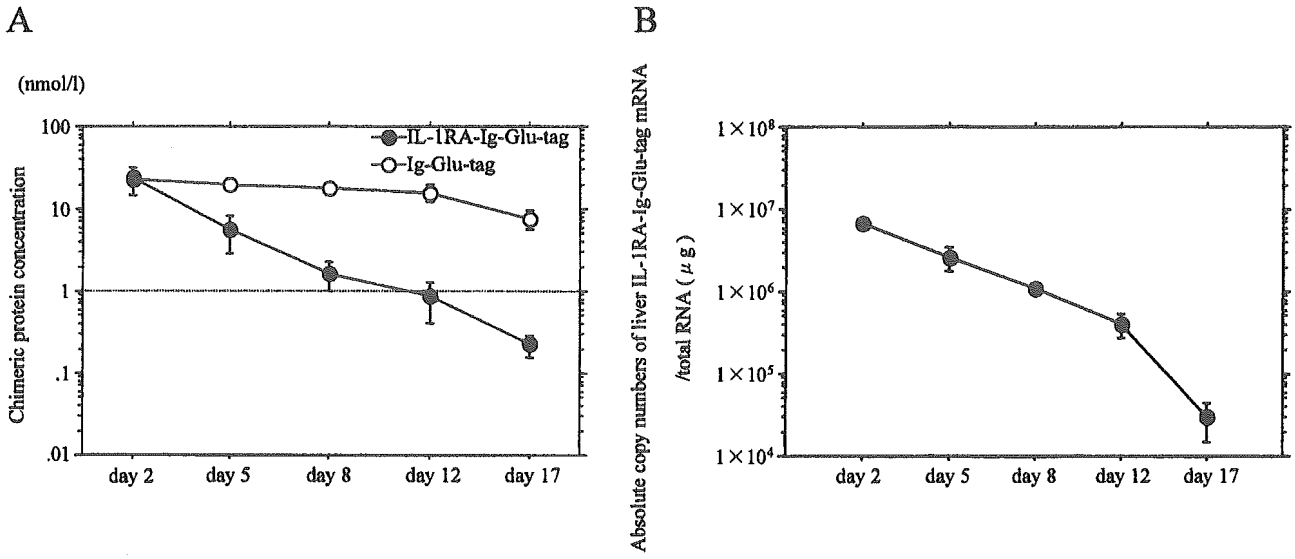

Figure 2. A, Plasma IL-1RA-Glu-tag protein and Ig-Glu-tag protein levels. Chimeric protein concentrations were calculated by use of Glu-tag. B, Absolute copy numbers of IL-1RA mRNA in liver (n=4). Error bars represent SEM. IL-1RA-Ig-Glu-tag indicates rats injected with pCAGGS-mouse IL-1RA-Ig-Glu-tag; Ig-Glu-tag, rats injected with pCAGGS-rat SP-Ig-Glu-tag.

to increase, peaking at 22.75±2.34 nmol/L on day 2, and gradually decrease to 19.48±1.62 nmol/L on day 5, 17.50±2.50 nmol/L on day 8, 15.59±3.56 nmol/L on day 12, and 7.45±1.88 nmol/L on day 17 (Figure 2A). The expressions of IL-1RA-Ig-Glu-tag transferred into normal rat liver by hydrodynamics-based gene delivery were similar to plasma IL-1RA-Ig-Glu-tag protein levels (Figure 2B). It has been reported that IL-1RA (1 to 10 ng/mL, 0.05 to 0.5 nmol/L) suppresses the production of PGES from rat astrocytes stimulated by lipopolysaccharide in vitro.[28] These results indicated that continuous effective delivery of IL-1RA-Ig protein for >16 days can be achieved in rats by hydrodynamics-based transfection.

Gene Expression of IL-1 Family in Purified Cells From EAM Hearts

Both IL-1α and IL-1β were strongly expressed in CD11b$^+$ cells. The IL-1RI gene was strongly expressed in NCNI cells (the cell fraction containing mainly fibroblasts, smooth muscle cells, and endothelial cells) and $\alpha\beta$T cells, whereas the IL-1RII gene was found to be markedly expressed in CD11b$^+$ cells. The IL-1Racp gene was strongly expressed in both CD11b$^+$ and NCNI cells and was moderately expressed in $\alpha\beta$T cells. Both total IL-1RA and sIL-1RA were detected in CD11b$^+$ cells. These results suggested that IL-1, produced mainly by CD11b$^+$ cells, acted on NCNI and $\alpha\beta$T cells by binding to IL-1RI and transduced intracellular signals by forming with IL-1Racp. On the other hand, CD11b$^+$ cells also produced native IL-1RA and IL-1RII, potentially suppressing the action of IL-1 (Figure 3).

Expression of Immunologic Molecules in Cultivated Cells With Serum Containing IL-1RA-Ig

IL-1RA-Ig–containing serum significantly reduced expression of PGES (mean±SEM, 1.22±0.22 versus 1.94±0.17; P<0.0001); Cox-2 (0.93±0.24 versus 2.00±1.05; P=0.0092), and IL-1β (3.91±1.22 versus 11.25±2.16; P<0.0001) at the mRNA level in cultivated NC cells (the cell fraction containing mainly fibroblasts, smooth muscle cells, and CD11b$^+$ cells) (Figure 4). In addition, IL-1RA-Ig–containing serum significantly reduced expression of the IL-2 (0.0004±0.0001 versus 0.0310±0.0090; P<0.0001) and IFN-γ (0.0065±0.0036 versus 0.0461±0.0385; P=0.0091) genes in cultivated lymphocytes (Figure 5).

Discussion

In the present study, we demonstrated that hydrodynamics-based delivery of plasmid DNA encoding the IL-1RA-Ig gene ameliorated EAM. IL-1RA-Ig–affecting cells were thought to be NCNI cells (fibroblasts, smooth muscle cells, and endothelial cells) and $\alpha\beta$T cells because IL-1RI and IL-1Racp were found in them. Endogenous IL-1α and IL-1β produced mainly by CD11b$^+$ cells, especially secreted IL-1β, influence these surrounding cells in a paracrine manner. IL-1RA-Ig, generated after gene transfer, appears to inhibit the IL-1–induced reactions of these cells and ameliorates EAM.

The functions of IL-1 with respect to cell regulation are varied.[29] In this study, the effect of serum containing IL-1RA-Ig on the mRNA expression of various immunologic molecules in cultivated NC cells (mainly fibroblasts, smooth muscle cells, and CD11b$^+$ cells) from hearts and lymphocytes from popliteal lymph nodes of EAM rats was investigated. The concentration of IL-1RA-Ig in cultivated cells was almost the same as that observed at the onset of myocarditis (day 10 to 11) and that reported by previous in vitro studies to be an effective dose.[28,30] In this study, there was a 30- to 50-fold increase in the expression of PGES, Cox-2, and IL-1β mRNA in NC cells by IL-1 alone, but the increase was significantly reduced by serum containing IL-1RA-Ig. PGE2 produced by PGES plays an important role in inflammation and pain.[31] In rheumatoid arthritis, the level of PGES detected

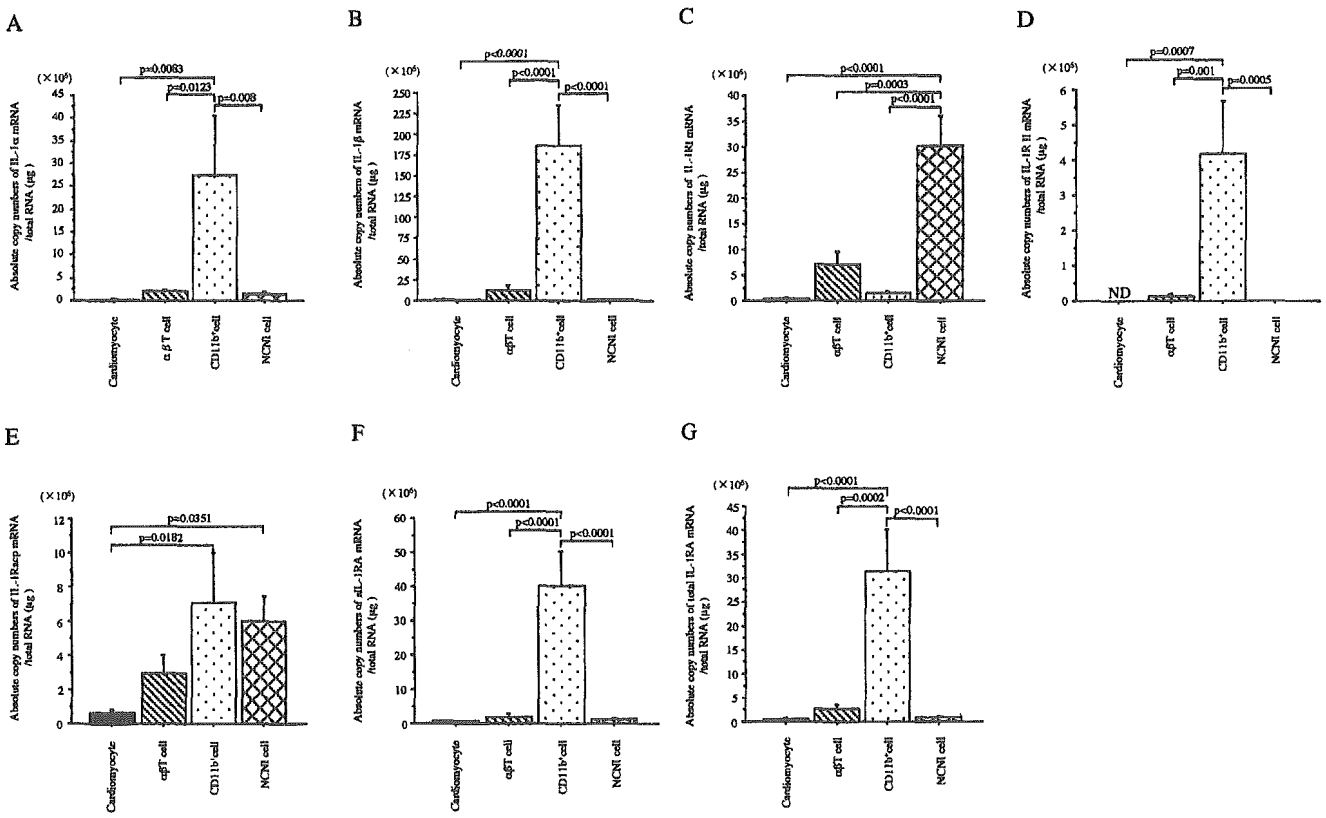

Figure 3. A through G, Absolute copy numbers of IL-1α, IL-1β, IL-1RI, IL-1RII, IL-1Racp, sIL-1RA, and total IL-1RA, respectively. Each cell was separated and purified from EAM heart on day 18. Error bars represent SEM. Statistical assessment was performed by 1-way ANOVA and Bonferroni multiple comparison test. Differences were considered significant at $P<0.05$.

at the inflammatory region is very high.[32] Our study of PGES and Cox-2 gene expression in purified cells from EAM hearts indicated that they were produced mainly by NCNI cells and slightly by CD11b$^+$ cells (data not shown). IL-1RA-Ig may inhibit the expression of the PGES and Cox-2 gene directly on NCNI cells via IL-1R. IL-1–induced IL-1 production has been shown in various cell types.[33] IL-1RA-Ig may also inhibit IL-1 production directly on NCNI cells. However, because our study indicated that IL-1 was produced mainly by CD11b$^+$ cells, IL-1RA-Ig may inhibit IL-1 production of CD11b$^+$ cells indirectly via NCNI cells or $\alpha\beta$T cells. Reduced PGES, Cox-2, and/or IL-1 production by NC cells in EAM hearts may be an effect resulting in improved myocarditis. On the other hand, in lymphocytes of popliteal lymph node, IL-2 and IFN-γ mRNA expression levels were significantly reduced by serum containing IL-1RA-Ig. In EAM,

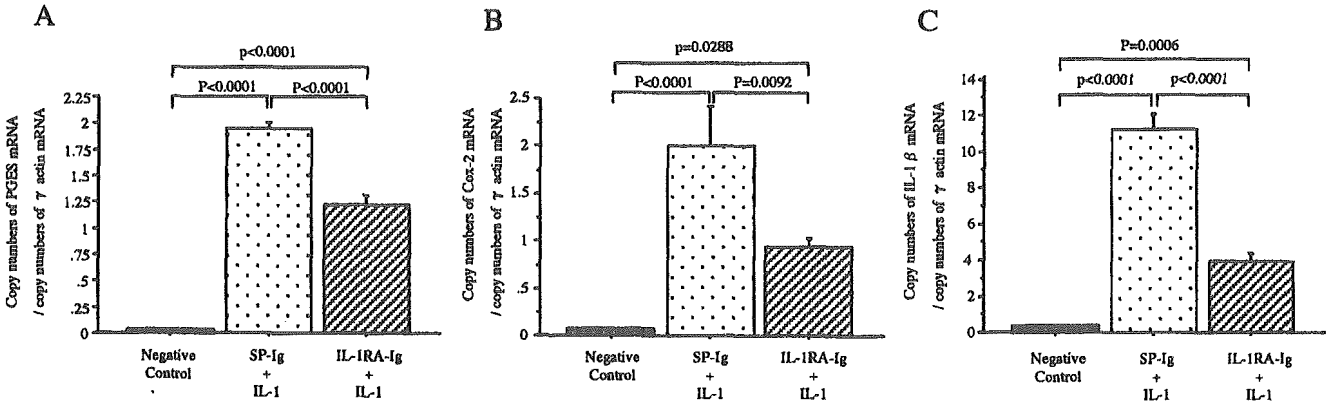

Figure 4. Copy numbers of various immunologic molecules mRNA/copy numbers of γ-actin mRNA in NC cells cultivated from EAM hearts. A, PGES; B, Cox-2; C, IL-1β. Negative control cells were cultivated in medium without IL-1α and rat serum. SP-Ig+IL-1 cells were cultivated in medium with IL-1α and rat serum treated with pCAGGS-SP-Ig-Glu-tag; IL-1RA-Ig+IL-1 cells were cultivated in medium with IL-1α and rat serum treated with pCAGGS-mouse IL-1RA-Ig-Glu-tag. Error bars represent SEM. Statistical assessment was performed by 1-way ANOVA and Bonferroni multiple comparison test. Differences were considered significant at $P<0.05$.

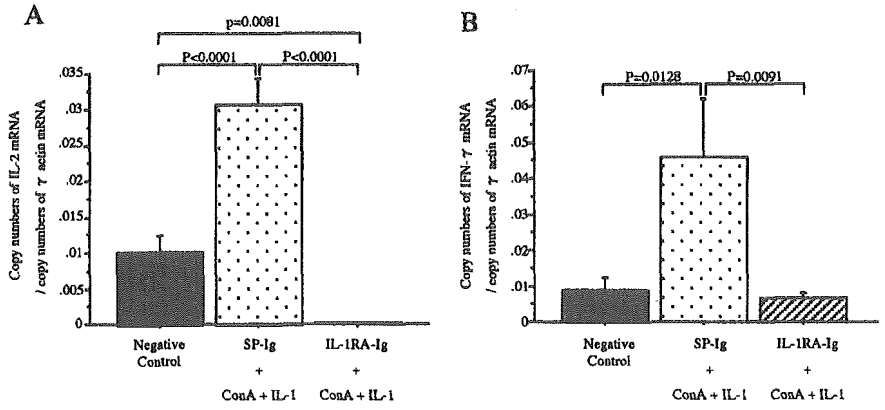

Figure 5. Copy numbers of various immunologic molecules mRNA/copy numbers of γ-actin mRNA in cultivated lymphocytes from swollen lymph node of EAM. A, IL-2; B, IFN-γ. Negative control cells were cultivated in medium without Con-A, IL-1α, and serum. SP-Ig+Con-A+IL-1 cells were cultivated in medium with Con-A, IL-1α, and rat serum treated with pCAGGS-SP-Ig-Glu-tag. IL-1RA-Ig+Con-A+IL-1 cells were cultivated in medium with Con-A, IL-1α, and rat serum treated with pCAGGS-mouse IL-1RA-Ig-Glu-tag. Error bars represent SEM. Statistical assessment was performed by 1-way ANOVA and Bonferroni multiple comparison test. Differences were considered significant at $P<0.05$.

which is a T cell–mediated disease,[27] Th1 cytokines such as IL-2 and IFN-γ produced by $CD4^+$ T cells are thought to play a central role.[4] Therefore, inhibition of Th1 cytokine production by IL-1RA-Ig may improve EAM.

In human rheumatoid arthritis, it has been reported that Anakinra (a recombinant form of IL-1RA) suppressed progression of this disease,[34] and treatment with IL-1RA has been investigated in various animal models.[16–18] Therefore, the number of diseases in which IL-1RA has a therapeutic relevance may be extended in the near future. Human myocarditis is serious and often fatal despite intensive care. However, the cause of myocarditis is not usually evident. It was reported that gene therapy with IL-1RA expression plasmid was effective in the treatment of viral myocarditis and reduced virus titer in hearts.[18] Here, we demonstrated that IL-1RA-Ig gene transfer ameliorated EAM resembling human giant cell myocarditis. Therefore, treatment with IL-1RA may be effective for acute and fulminant myocarditis even if its cause is unknown.

Hydrodynamics-based gene delivery of plasmid DNA as used in this study is both inexpensive and highly effective in terms of facilitating gene expression. The concentration of IL-1RA-Ig in blood obtained by this method was higher compared with plasmid DNA transfection into muscle with in vivo electroporation.[19,20] The producing cells to which plasmid DNA is transferred by this method are thought to be mainly hepatocytes. Plasmid DNA is thought to be delivered into hepatocytes by retrograde blood flow from hepatic veins. If plasmid DNA encoding IL-1RA-Ig can be directly transfected into the heart, T cells and NCNI cells in EAM hearts will be highly influenced by IL-1RA-Ig, and EAM may be ameliorated. Hou et al[35] reported heart-targeted plasmid DNA transfer by retrograde coronary vein using a balloon catheter. This method, which is easy and not very risky, may be suitable for human clinical application. New developments of this gene therapy can be expected in the future.

References

1. Kodama M, Matsumoto Y, Fujiwara M, Masani F, Izumi T, Shibata A. A novel experimental model of giant cell myocarditis induced in rats by immunization with cardiac myosin fraction. *Clin Immunol Immunopathol.* 1990;57:250–262.
2. Kodama M, Hanawa H, Saeki M, Hosono H, Inomata T, Suzuki K, Shibata A. Rat dilated cardiomyopathy after autoimmune giant cell myocarditis. *Circ Res.* 1994;75:278–284.
3. Kodama M, Zhang S, Hanawa H, Shibata A. Immunohistochemical characterization of infiltrating mononuclear cells in the rat heart with experimental autoimmune giant cell myocarditis. *Clin Exp Immunol.* 1992;90:330–335.
4. Hanawa H, Abe S, Hayashi M, Yoshida T, Yoshida K, Shiono T, Fuse K, Ito M, Tachikawa H, Kashimura T, Okura Y, Kato K, Kodama M, Maruyama S, Yamamoto T, Aizawa Y. Time course of gene expression in rat experimental autoimmune myocarditis. *Clin Sci (Lond).* 2002;103:623–632.
5. March CJ, Mosley B, Larsen A, Cerretti DP, Braedt G, Price V, Gillis S, Henney CS, Kronheim SR, Grabstein K. Cloning, sequence and expression of two distinct human interleukin-1 complementary DNAs. *Nature.* 1985;315:641–647.
6. Scala G, Allavena P, Djeu JY, Kasahara T, Ortaldo JR, Herberman RB, Oppenheim JJ. Human large granular lymphocytes are potent producers of interleukin-1. *Nature.* 1984;309:56–59.
7. Rupp EA, Cameron PM, Ranawat CS, Schmidt JA, Bayne EK. Specific bioactivities of monocyte-derived interleukin 1 alpha and interleukin 1 beta are similar to each other on cultured murine thymocytes and on cultured human connective tissue cells. *J Clin Invest.* 1986;78:836–839.
8. Baldari C, Murray JA, Ghiara P, Cesareni G, Galeotti CL. A novel leader peptide which allows efficient secretion of a fragment of human interleukin-1 beta in Saccharomyces cerevisiae. *EMBO J.* 1987;6:229–234.
9. Sims JE, Acres RB, Grubin CE, McMahan CJ, Wignall JM, March CJ, Dower SK. Cloning the interleukin 1 receptor from human T cells. *Proc Natl Acad Sci U S A.* 1989;86:8946–8950.
10. Wesche H, Korherr C, Kracht M, Falk W, Resch K, Martin MU. The interleukin-1 receptor accessory protein (IL-1RAcP) is essential for IL-1–induced activation of interleukin-1 receptor–associated kinase (IRAK) and stress-activated protein kinases (SAP kinases). *J Biol Chem.* 1997;272:7727–7731.
11. Colotta F, Re F, Muzio M, Bertini R, Polentarutti N, Sironi M, Giri JG, Dower SK, Sims JE, Mantovani A. Interleukin-1 type II receptor: a decoy target for IL-1 that is regulated by IL-4. *Science.* 1993;261:472–475.
12. Arend WP, Malyak M, Guthridge CJ, Gabay C. Interleukin-1 receptor antagonist: role in biology. *Annu Rev Immunol.* 1998;16:27–55.
13. McIntyre KW, Stepan GJ, Kolinsky KD, Benjamin WR, Plocinski JM, Kaffka KL, Campen CA, Chizzonite RA, Kilian PL. Inhibition of interleukin-1 (IL-1) binding and bioactivity in vitro and modulation of acute inflammation in vivo by IL-1 receptor antagonist and anti-IL-1 receptor monoclonal antibody. *J Exp Med.* 1991;173:931–939.
14. Dinarello CA. The interleukin-1 family: 10 years of discovery. *FASEB J.* 1994;8:1314–1325.
15. Guo C, Dower SK, Holowka D, Baird B. Fluorescence resonance energy transfer reveals interleukin (IL)-1–dependent aggregation of IL-1 type I receptors that correlates with receptor activation. *J Biol Chem.* 1995;270:27562–27568.
16. Badovinac V, Mostarica-Stojkovic M, Dinarello CA, Stosic-Grujicic S. Interleukin-1 receptor antagonist suppresses experimental autoimmune encephalomyelitis (EAE) in rats by influencing the activation and proliferation of encephalitogenic cells. *J Neuroimmunol.* 1998;85:87–95.
17. Kim JM, Jeong JG, Ho SH, Hahn W, Park EJ, Kim S, Yu SS, Lee YW, Kim S. Protection against collagen-induced arthritis by intramuscular gene therapy with an expression plasmid for the interleukin-1 receptor antagonist. *Gene Ther.* 2003;10:1543–1550.

18. Nakano A, Matsumori A, Kawamoto S, Tahara H, Yamato E, Sasayama S, Miyazaki JI. Cytokine gene therapy for myocarditis by in vivo electroporation. *Hum Gene Ther.* 2001;12:1289–1297.
19. Maruyama H, Higuchi N, Nishikawa Y, Kameda S, Iino N, Kazama JJ, Takahashi N, Sugawa M, Hanawa H, Tada N, Miyazaki J, Gejyo F. High-level expression of naked DNA delivered to rat liver via tail vein injection. *J Gene Med.* 2002;4:333–341.
20. Liu F, Song YK, Liu D. Hydrodynamics-based transfection in animals by systemic administration of plasmid DNA. *Gene Therapy.* 1999;6: 1258–1266.
21. Jiang J, Yamato E, Miyazaki J. Sustained expression of Fc-fusion cytokine following in vivo electroporation and mouse strain differences in expression levels. *J Biochem (Tokyo).* 2003;133:423–427.
22. Nishino T, Kodaira T, Shin S, Imagawa K, Shima K, Kumahara Y, Yanaihara C, Yanaihara N. Glucagon radioimmunoassay with use of antiserum to glucagon C-terminal fragment. *Clin Chem.* 1981;27: 1690–1697.
23. Hanawa H, Watanabe R, Hayashi M, Yoshida T, Abe S, Komura S, Liu H, Elnaggar R, Chang H, Okura Y, Kato K, Kodama M, Maruyama H, Miyazaki J, Aizawa Y. A novel method to assay proteins in blood plasma after intravenous injection of plasmid DNA. *Tohoku J Exp Med.* 2004; 202:155–161.
24. Hwang TC, Horie M, Nairn AC, Gadsby DC. Role of GTP-binding proteins in the regulation of mammalian cardiac chloride conductance. *J Gen Physiol.* 1992;99:465–489.
25. Isenberg G, Klockner U. Calcium tolerant ventricular myocytes prepared by preincubation in a "KB medium." *Pflugers Arch.* 1982;395:6–18.
26. Toba K, Hanawa H, Fuse I, Sakaue M, Watanabe K, Uesugi Y, Higuchi W, Takahashi M, Aizawa Y. Difference in CD22 molecules in human B cells and basophils. *Exp Hematol.* 2002;30:205–211.
27. Kodama M, Matsumoto Y, Fujiwara M. In vivo lymphocyte-mediated myocardial injuries demonstrated by adoptive transfer of experimental autoimmune myocarditis. *Circulation.* 1992;85:1918–1926.
28. Pistritto G, Ciabattoni G, Mancuso C, Tringali G, Preziosi P, Navarra P. Signaling pathways involved in lipopolysaccharide stimulation of prostaglandin production by rat hypothalamic astroglial cells. *J Endotoxin Res.* 2000;6:307–311.
29. Dinarello CA. Interleukin-1 and interleukin-1 antagonism. *Blood.* 1991; 77:1627–1652.
30. Rambaldi A, Torcia M, Dinarello CA, Barbui T, Cozzolino F. Modulation of cell proliferation and cytokine production in AML by recombinant interleukin-1 receptor antagonist. *Leukemia.* 1993;7:S10–S12.
31. Trebino CE, Stock JL, Gibbons CP, Naiman BM, Wachtmann TS, Umland JP, Pandher K, Lapointe JM, Saha S, Roach ML, Carter D, Thomas NA, Durtschi BA, McNeish JD, Hambor JE, Jakobsson PJ, Carty TJ, Perez JR, Audoly LP. Impaired inflammatory and pain responses in mice lacking an inducible prostaglandin E synthase. *Proc Natl Acad Sci U S A.* 2003;100:9044–9049.
32. Stichtenoth DO, Thoren S, Bian H, Peters-Golden M, Jakobsson PJ, Crofford LJ. Microsomal prostaglandin E synthase is regulated by proinflammatory cytokines and glucocorticoids in primary rheumatoid synovial cells. *J Immunol.* 2001;167:469–474.
33. Warner SJ, Auger KR, Libby P. Human interleukin 1 induces interleukin 1 gene expression in human vascular smooth muscle cells. *J Exp Med.* 1987;165:1316–1331.
34. Fleischmann RM. Addressing the safety of anakinra in patients with rheumatoid arthritis. *Rheumatology (Oxford).* 2003;42:ii29–ii35.
35. Hou D, Maclaughlin F, Thiesse M, Panchal VR, Bekkers BC, Wilson EA, Rogers PI, Coleman MC, March KL. Widespread regional myocardial transfection by plasmid encoding Del-1 following retrograde coronary venous delivery. *Catheter Cardiovasc Interv.* 2003;58:207–211.

Available online at www.sciencedirect.com

SCIENCE DIRECT®

Comparative Biochemistry and Physiology, Part B 142 (2005) 153 – 163

CBP

www.elsevier.com/locate/cbpb

Expression and tissue distribution of astacin-like squid metalloprotease (ALSM)

Nobuyuki Kanzawa*, Shuntaro Tatewaki, Ryousuke Watanabe, Ikuko Kunihisa, Haruka Iwahashi, Kaori Nakamura, Takahide Tsuchiya

Department of Chemistry, Faculty of Science and Technology, Sophia University, 102-8554, Tokyo, Japan

Received 28 January 2005; received in revised form 14 May 2005; accepted 15 May 2005
Available online 2 August 2005

Abstract

Astacin metalloprotease family members function in a wide variety of biologic events, including cell differentiation and morphogenesis during embryonic development and adult tissue differentiation. We previously isolated and characterized an astacin-like squid metalloprotease (ALSM). To elucidate the embryonic expression of ALSM, we performed immunohistochemical analysis with specific antibodies and examined the expression profiles of ALSM isoforms by in situ hybridization analysis. Tissue distribution and expression were also examined in adult spear squid. mRNA expression of ALSM isoforms I and III was first detected in newly hatched squid and was restricted to the liver. No mRNA signals were detected in other tissues even in adult squids. At the protein level, both isoforms were prominent in the liver of embryos and later in digestive organs of adult squid. Both isoforms were also detected in muscle tissues, including mantle and tentacle muscle. Staining for ALSM III was also identified in the iris and in tissues near the eye in squid embryos. However, no reactive bands were detected by immunoblotting of adult squid eyes. Thus, ALSM is initially expressed at the late stage of embryogenesis in spear squid, and expression is restricted to the liver. Thereafter, ALSM isoforms function in various tissues in an isoform-dependent manner.

Keywords: ALSM; Astacin; Embryo; Expression; Liver; Metalloprotease; Squid; Tissue distribution

1. Introduction

Astacin-like squid metalloprotease (ALSM) has a high substrate specificity for myosin heavy chain (MyHC) and was originally identified in squid mantle muscle (Okamoto et al., 1993; Tamori et al., 1999). Primary sequence analysis has shown that ALSM is a member of the astacin family (Yokozawa et al., 2002). Astacins were first identified as digestive enzymes (EC 3.4.24.21) in the stomach of the freshwater crayfish *Astacus astacus* (Titani et al., 1987; Dumermuth et al., 1991). Astacin family members have unique consensus sequences, including a zinc-binding sequence (HEXXHXXGFXHEXXRXDRD) and a Met-turn sequence (SXMHY) (Bode et al., 1993), and have been identified in various organisms from mammals to hydras (Bond and Beynon, 1995; Sarras, 1996). Studies of domain structure have revealed that astacins possess signal and prosequence domains along with a conserved protease domain characterized by the zinc-binding motif as well as a unique C-terminal domain specific to each family member. ALSM possesses signal, prosequence, and protease domains, followed by a MAM (meprin, A5 protein, receptor protein-tyrosine phosphatase μ) domain, which is a conserved domain in the C-terminus of meprin, an astacin family member (Bond and Beynon, 1995; Yokozawa et al., 2002). Astacins are involved in a wide variety of physiologic events, including digestion (Vogt et al., 1989), development (Takahara et al., 1994; Piccolo et al., 1996), hatching (Yasumasu et al., 1992a; Lee et al., 1994; Katagiri et al., 1997; Fan and Katagiri, 2001), regeneration (Yan et al., 2000a,b), and activation of hormones and some peptides (Yamaguchi et al., 1991). For example, human bone

* Corresponding author. Tel.: +81 3 3238 3363; fax: +81 3 3238 3361.
E-mail address: n-kanza@sophia.ac.jp (N. Kanzawa).

1096-4959/$ - see front matter © 2005 Elsevier Inc. All rights reserved.
doi:10.1016/j.cbpc.2005.05.018

morphogenetic protein 1 (huBMP1) induces ectopic bone formation in adult vertebrates (Wozney et al., 1988); *Drosophila* tolloid is required for normal dorsal patterning (Shimell et al., 1991; Marques et al., 1997); and meprins are found in mammalian kidney and intestinal tissues and play crucial roles in the processing of biologically active peptides and extracellular matrix (ECM) proteins (Craig et al., 1987; Bond and Beynon, 1995). An astacin-like protein from the freshwater polyp *Hydra vulgaris*, described as hydra metalloprotease I (HMP-1), is localized in the ECM in a head-specific manner and has a functional role during development (Yan et al., 1995). The fish hatching enzymes, high and low choriolytic enzymes (HCE/LCE), are secreted from hatching glands and digest the egg envelope (Yasumasu et al., 1992b; Inohaya et al., 1995). Thus, astacins have unique functions in each tissue in which they are expressed. ALSM can hydrolyze MyHC; therefore, it is thought to be involved in the metabolism of skeletal muscle proteins (Okamoto et al., 1993). Tissue distribution analysis of ALSM activity with the use of MyHC as an in vitro substrate revealed that ALSM exists in a wide variety of tissues, particularly in digestive organs (Tajima et al., 1998; Tamori et al., 1999). Two groups of ALSM isoforms are present in squid: types I and III in spear squid and types I and II in Japanese common squid. These isoforms are classified according to specificity for hydrolytic sites in rabbit skeletal muscle MyHC. Differentially regulated expression and distribution of the two groups of astacins have been reported in hydra (Yan et al., 2000a,b). However, the exact expression profiles of astacin isoforms have not been reported.

In the present study, we obtained specific antibodies for ALSM I and III isolated from spear squid (*Loligo bleekeri*) and examined the tissue distributions of ALSM isoforms in squid by immunohistochemistry. Expression of ALSM mRNA in the squid was examined by in situ hybridization and northern blotting and RT-PCR analysis.

2. Materials and methods

2.1. Materials

Spear squid (*Loligo bleekeri*) were purchased from the Tokyo Central Wholesale Fish Market. Spear squid eggs and embryos were a kind gift from Dr. Yuzuru Ikeda, Ryukyu University, and were fixed immediately in 4% paraformaldehyde for histochemical and immunohistochemical analyses or frozen in liquid nitrogen for biochemical analysis. Embryos were collected from eggs incubated in a small aquarium after approximately 6, 8, and 10 weeks of incubation. Eggs incubated for 6 or 8 weeks were extracted from the egg capsules, and the embryos were removed from the eggs. Embryos after 10 weeks of incubation were at the hatching stage. Embryos were inspected under light microscopy (Fig. 1), and embryonic stages were determined on the basis of morphologic characteristics according to the criteria of Baeg et al. (1992). Embryos after 6 weeks of incubation had large yolk sacs compared to the embryonic body; red retinas and red chromatophores were evident on the mantle surface but not on the tentacles, as is typical of stage 23 of embryonic development. In embryos after 8 weeks of incubation, the yolk sac and head were approximately the same size, which is typical of stage 26. Another marker of this stage, a filled ink sac, was also visible through the mantle muscle. Newly hatched embryos were classified as stage 28 embryos.

2.2. Expression of recombinant proteins

Recombinant ALSM I and III of spear squid were expressed in *Escherichia coli* for antibody specificity tests. ALSM I and III cDNAs were amplified from isolated clones (Yokozawa et al., 2002) by PCR with primer pairs (summarized in Table 1) of Y1-20 and T3 primer, and Y3-1 and Y3-2, respectively. Amplified fragments were

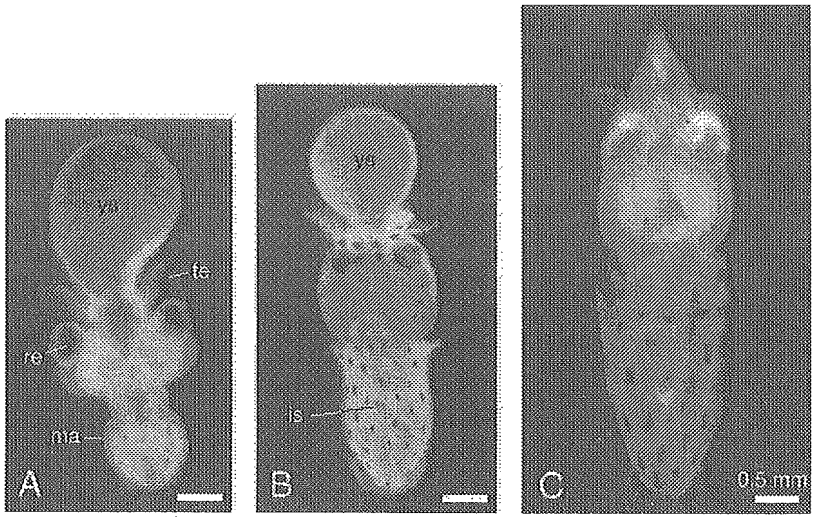

Fig. 1. Light micrographs of spear squid embryos at stages 23 (A), 26 (B), and 28 (C) is, ink sac; ma, mantle; re, retina; te, tentacle; ys, yolk sac.

Table 1
Oligonucleotide primers used for PCR amplification

Target gene	Primer name	Direction	Sequence
Spear squid (Loligo bleekeri)			
ALSM I	Y1-20	forward:	5′-CCATGGCTGTACCTCTGGACACCGAGC-3′
	Y1-15	reverse:	5′-CCGGATCCTTAACATTTTCCATC-3′
ALSM I	Y1-7	forward:	5′-GGGCATATGCTGGGTGGTGGATGTCGTG-3′
	Y1-12	reverse:	5′-GAATTCTCATGAATTGTAATCGTA-3′
ALSM III	Y3-1	forward:	5′-GGATCCATGGCAAACGCAATTGGTAATCTCAAA-3′
	Y3-2	reverse:	5′-GGATCCATGGCACAACTTCCAGGTGTAAGTAAA-3′
ALSM III	Y3-h	forward:	5′-GGTCTTCCATATGATTACAATTC-3′
	Y3-t	reverse:	5′-TCATCTGTTTCCATTTATTTCCTT-3′
actin	Actin-f	forward:	5′-TCTGGCACCACACCTTCTACA-3′
	Actin-r	reverse:	5′-GCCACGTAGCACAGCTTCTC-3′
Japanese common squid (Todarodes pacificus)			
ALSM I	S1-1	forward:	5′-GGATCCATGGCAAGTGTTGTTGGAGATCTTAAC-3′
	S1-2	reverse:	5′-GGATCCATGGCGCATCTTCCATCCAGAATAAA-3′
ALSM II	S2-1	forward:	5′-GGATCCATGGCAAACGCAGTTGGTAGCATCAAA-3′
	S2-2	reverse:	5′-GGATCCATGGCACATTT CCCAGGCGTAAGTACG-3′

then ligated into the pGEM-T Easy Vector (Promega, Madison, WI, USA). An insert of ALSM I containing sequence for the propeptide, protease, and MAM domains was digested with *Nco*I/*Eco*RI and further ligated into the expression vector pET32b (Novagen, Madison WI, USA) to express a thioredoxin-fused protein (65 kDa). An insert of ALSM III containing the protease and MAM domains was digested with *Nco*I enzyme and ligated into the *Nco*I site of the expression vector pETGEX-CT (Sharrocks, 1994) provided from the Department of Microbial Genetics, National Institute of Genetics (Shizuoka, Japan), and the direction was determined by sequencing of isolated clones. *E. coli* (BL21) were transformed with isolated clones, and expression of glutathione-*S*-transferase (GST)-fused protein (62 kDa) was induced by 1 mM IPTG.

Recombinant ALSM I and II from Japanese common squid (*Todarodes pacificus*) were also expressed in *E. coli* for use in antibody specificity tests. ALSM I and II were amplified with primer pairs of S1-1 and S1-2, and S2-1 and S2-2, respectively. Both amplified fragments were ligated into the pGEM-T Easy Vector and then subclone into the pETGEX-CT expression vector. Ligation and transformation of *E. coli* were performed by the same technique as that for spear squid ALSM III. The relative molecular masses of GST-fused proteins of Japanese common squid ALSM I and II were 62 kDa and 65 kDa, respectively.

2.3. Antibody generation and immunoblot analysis

The polyclonal antibody (TY-ID) generated against a small peptide from spear squid ALSM I was characterized previously (Yokozawa et al., 2002). To generate an antibody against spear squid ALSM III, GST-fused ALSM III was expressed in *E. coli* as described above, purified on glutathione-agarose beads according to the manufacturer's instructions (Amersham Pharmacia Biotech, Little Chalfont, UK), and cleaved with 1 unit/L thrombin (Sigma-Aldrich Chemical Co., St. Louis, MO, USA). Cleaved ALSM III with protease and MAM domains was resolved by sodium dodecyl sulfate polyacrylamide gel electrophoresis (SDS-PAGE) (Laemmli, 1970) followed by electrophoretic elution of ALSM III peptide from the gels. The purified peptide was dialyzed against phosphate-buffered saline (PBS) and used as antigen. Rabbits were immunized with the antigen emulsified in Freund's complete adjuvant and were boosted twice with the same antigen emulsified in Freund's incomplete adjuvant. Serum containing anti-ALSM III antibody was purified by incubating the serum with nitrocellulose-bound antigen and then eluting it at low pH (Sambrook et al., 1989). Purified antibody to ALSM III was designated as KY-III.

To confirm the specificity of the generated antibodies, crude liver extracts of adult spear squid were incubated with antibody and protein A-Sepharose (Amersham Pharmacia Biotech). Immune complex was washed three times with PBS and divided into the half. One was eluted by the SDS-sample solution (10% glycerol, 10% 2-mercaptoethanol, 3% SDS, and 62.5 mM Tris–HCl, pH 6.7) and then was resolved by 12% SDS-PAGE. The other half was incubated with rabbit skeletal muscle myosin to examine the enzyme activity (Tamori et al., 1999). Briefly, immune complex was mixed with reaction mixture to give final concentrations of 0.6 mg/mL rabbit skeletal muscle myosin, 100 mM sodium phosphate, pH 7.2, 5 mM EDTA, 4 mM MIA, 8 mM phenylmethylsulphonyl fluoride (PMSF), 20 μg/mL pepstatin A, 20 μg/mL leupeptin, and 10 mM $ZnCl_2$. After incubation for overnight at 37 °C, the reaction was stopped by addition of SDS sample solution. Aliquots of the sample were subjected to 10% SDS-PAGE.

2.4. Tissue sectioning and immunohistochemistry

Spear squid embryos fixed in paraformaldehyde were rinsed with PBS several times and frozen in Tissue-Tek

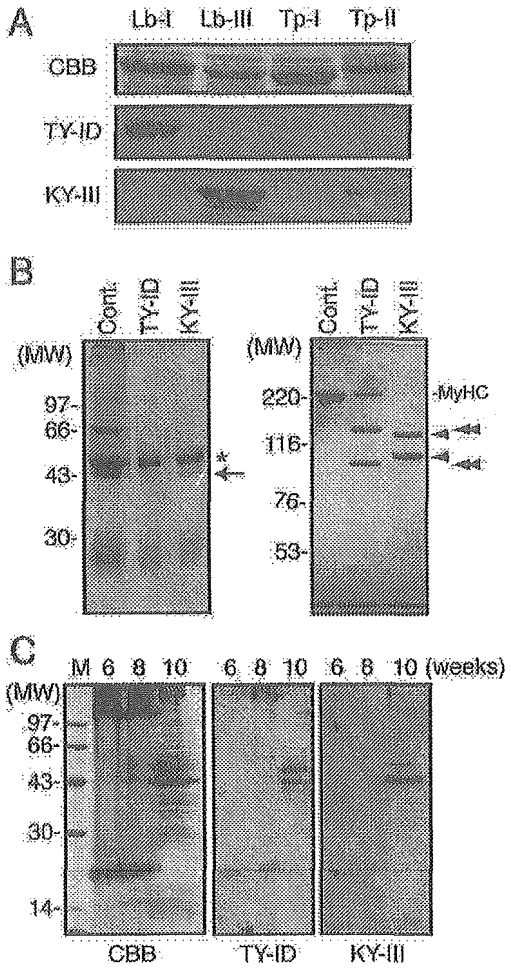

Fig. 2. Specificity tests of antibodies against ALSM isoforms. A, Lb-I and Lb-III, *Loligo bleekeri* ALSM I and III. Tp-I and Tp-II, *Todarodes pacificus* ALSM I and II. Bacterially expressed isoforms were subjected to SDS-PAGE and either stained with Coomassie Brilliant Blue (CBB) (top panel) or detected with antibodies to ALSM I (TY-ID) or III (KY-III). B, Crude liver extracts of adult spear squid were incubated with pre-immune serum (Cont.), TY-ID and KY-III, and precipitated with protein A-Sepharose. Precipitates were eluted and resolved by SDS-PAGE (left panel). Asterisk shows the major band of antibody heavy chain. Arrow represents the molecular size of ALSMs. Enzyme activity was examined with the precipitates (right panel). No hydrolysis of rabbit skeletal muscle heavy chain (MyHC) was observed in control; however, 130 and 90 kDa fragments (arrowheads), and 120 and 100 kDa fragments (double-arrowheads) were observed when rabbit myosin was incubated with immunoprecipitate with TY-ID and KY-III, respectively. C, Immunoblot analysis of ALSM isoforms in spear squid embryos incubated 6 (stage 23), 8 (stage 26), and 10 (stage 28) weeks. Approximately 10 μg of total protein from each sample extract was subjected to SDS-PAGE followed by staining with CBB or detection with antibodies to ALSM isoforms. Both ALSM I (TY-ID) and III (KY-III) were detected in extracts of stage 28 embryos as a doublet. No signals were detected at other embryonic stages.

OCT compound (Miles, Elkhart, IN, USA) or mounted in low-melt wax as follows: Embryos were dehydrated in a graded ethanol/PBS series (30%, 50%, 70%, 90%, and 100% ethanol), 1 h per step at 4 °C. After two incubations in 100% ethanol, the specimens were stored at 4 °C overnight. Embedding was carried out at 37 °C, first for 30 min in 100% ethanol at 37 °C, then in a graded 100% ethanol/low-melt wax (Steedman, 1957) series (2:1, 1:1, 1:2 *v/v*) followed by three changes of pure wax, each for 1–2 h, and overnight incubation at 37 °C. Specimens were then placed into embedding molds and left to polymerize overnight at room temperature. Ribbons of 10-μm sections were placed on albumin-coated slides and stretched by the addition of a small drop of distilled water to one end of the ribbon. For dewaxing and rehydration of sections, specimens were immersed in an ethanol/PBS series (100%, 70%, 50%, 30%, and 10% ethanol), 10 min per step at room temperature. After two incubations in PBS for 10 min each, the specimens were used for histochemical or immunohistochemical analysis.

Indirect immunofluorescence was performed as described previously (Yokozawa et al., 2002). Briefly, specimens were permeabilized at room temperature in 0.1% Triton X-100 for 5 min. After a washing with PBS, nonspecific binding was blocked with 10% normal goat serum and 3% bovine serum albumin (BSA) in PBS for 1 h. Double immunolabeling was performed with anti-actin antibody (diluted 1:2000, clone C4; ICN Pharmaceuticals Inc., Costa Mesa, CA, USA) and affinity purified polyclonal antibodies TY-ID or KY-III (diluted 1:100). The secondary antibodies were Alexa 594-conjugated goat anti-mouse IgG_1 antibody (diluted 1:150; Molecular Probes, Eugene, OR, USA) for the C4 antibody and fluorescein-labeled goat anti-rabbit IgG antibody (Kirkegaard and Perry Laboratories Inc., Gaithersburg, MD, USA) for the TY-ID and KY-III antibodies. Specimens were examined with a confocal microscope (LSM410; Carl Zeiss Inc., Oberkochen, Germany).

2.5. Analysis of ALSM III mRNA expression in embryonic tissue sections

To obtain sense and antisense riboprobes for ALSM I, a small fragment (250 bp) was PCR amplified with the primer pair of Y1-7 and Y1-12, and ligated into the pGEM-T Easy Vector. The obtained subclone was linearized and used as a template for the generation of riboprobes with a MAXIscript In Vitro Transcription Kit (Ambion Inc., Austin, TX, USA). Specificity of the probe was tested against clones of ALSM I and III (data not shown). In situ hybridization (Henrique et al., 1995) was performed as described previously (Takebayashi-Suzuki et al., 2000; Kanzawa et al., 2002). Briefly, sections prepared as described above were treated with 20 μg/mL proteinase K for 3 min at room temperature. After post-fixation with 4% paraformaldehyde in PBS for 10 min at room temperature, specimens were rinsed with PBS, preincubated with the hybridization mixture for 30 min at 65 °C, and reacted overnight at 65 °C with 0.5–1.0 μg/mL digoxigenin (DIG)-labeled riboprobe. After 60 °C washes and blocking, the samples were incubated overnight at 4 °C with alkaline phosphatase-conjugated anti-DIG antibody (diluted 1:2000, Roche, Switzerland). After washing to remove unbound antibody, samples were stained with NBT/BCIP mixture at room temperature for color development.

2.6. Northern blotting and RT-PCR analysis

Total RNA was extracted with TRIzol reagent (Invitrogen), and approximately 30 μg of total RNA was separated on a 1.0% agarose/formaldehyde gels and transferred to a Hybond-N+ membrane (Amersham). Probes for Northern hybridization were prepared as follows: Partial sequences were amplified from isolated clones by PCR with primer pairs of Y1-7 and Y1-12 for ALSM I, and Y3-h and Y3-t for ALSM III, and amplified fragments were ligated into pGEM-T Easy Vector. Insert digested with *Eco*RI was used as specific probe. Probe labeling, hybridization and detection were performed with the ECL Direct Nucleic Acid Labelling and Detection System (Amersham) according to the manufacturer's instructions.

RT-PCR was performed with total RNA as follows: After reverse transcription with oligo-dT primer, DNA was amplified using primers against each specific sequence; Y1-20 and Y1-15 for ALSM I, Y3-1 and Y3-2 for ALSM III, and actin-f and actin-r for actin. PCR reaction conditions for ALSM I and actin included initial denaturation for 2 min at 95 °C followed by 30 cycles at 95 °C for 45 s, 56 °C for 45 s, and 72 °C for 90 s each plus a final incubation for 3 min at 72 °C. PCR amplification for ALSM III was performed as described above except the annealing temperature was 58 °C. Yielded products of ALSM I, III, and actin were 1261bp, 1142 bp, and 406 bp, respectively. PCR products were resolved on 1% agarose gels and stained with 1 μg/mL ethidium bromide.

3. Results

3.1. Antibody specificity

To generate a specific antibody against ALSM III, recombinant protein containing the propeptide, protease, and MAM domains was used to immunize rabbits, and antibody was purified from the serum and designated as KY-III. To characterize the antibody specificity, immunoreactivity to bacterially expressed ALSMs was examined (Fig. 2A). TY-ID recognized ALSM I from spear squid (Lb-I) but not isoform from Japanese common squid (Tp-1). This is due to the difference in peptide sequence, which was used to generate TY-ID (Yokozawa et al., 2002). KY-III recognized ALSM III from spear squid (Lb-III) and, to a lesser extent, ALSM II from Japanese common squid (Tp-II). To certificate the specificity of antibodies, we performed immunoprecipitation experiments with the generated antibodies. The band of ALSM isoforms precipitated with antibodies was not confirmed clearly, because of the presence of antibody heavy chain at the similar molecular masses (Fig. 2B, left panel). However, precipitates exhibited specific activities to hydrolyze myosin heavy chain (Fig.

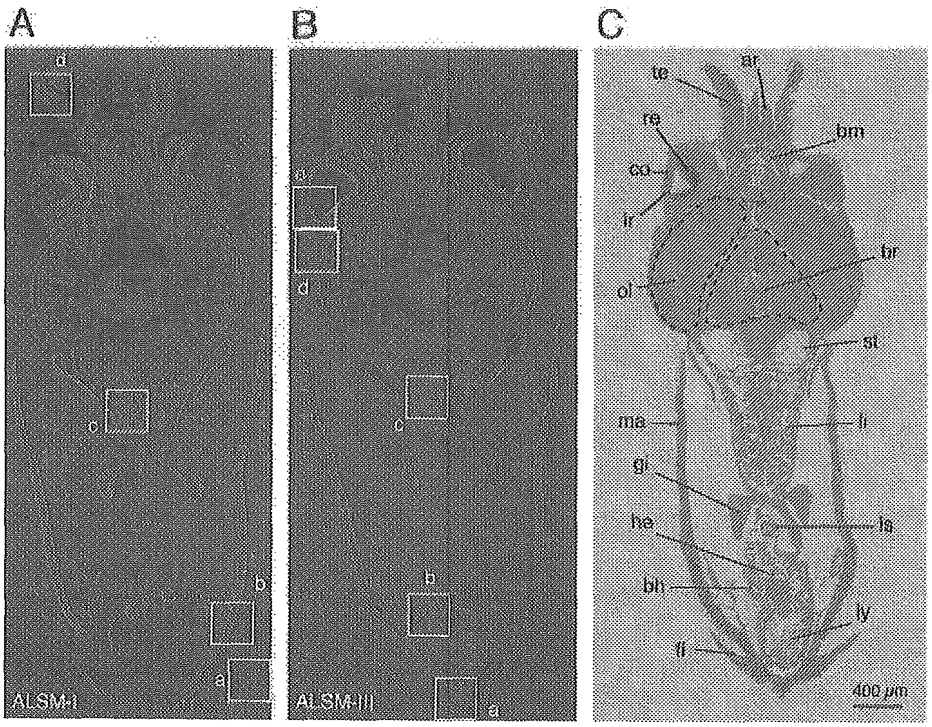

Fig. 3. Overview of the immunohistochemical distribution of ALSM isoforms in newly hatched squid (stage 28). Merged images were obtained by double immunostaining with specific antibodies against cellular actin (red) and ALSM isoforms (green), ALSM I (A), or III (B). White boxes (a–d in panel A and a–e in panel B) correspond to the panel numbers in Figs. 4 and 5, respectively. C, Light micrograph of a section of newly hatched squid (stage 28). ar, arm; bh, branchial heart; bm, buccal mass; br, brain; co, cornea; fi, fin; gi, gill; he, heart; is, ink sac; ir, iris; iy, inner yolk; li, liver; ma, mantle; ol, optic lobe; re, retina; st, statocyst; te, tentacle.

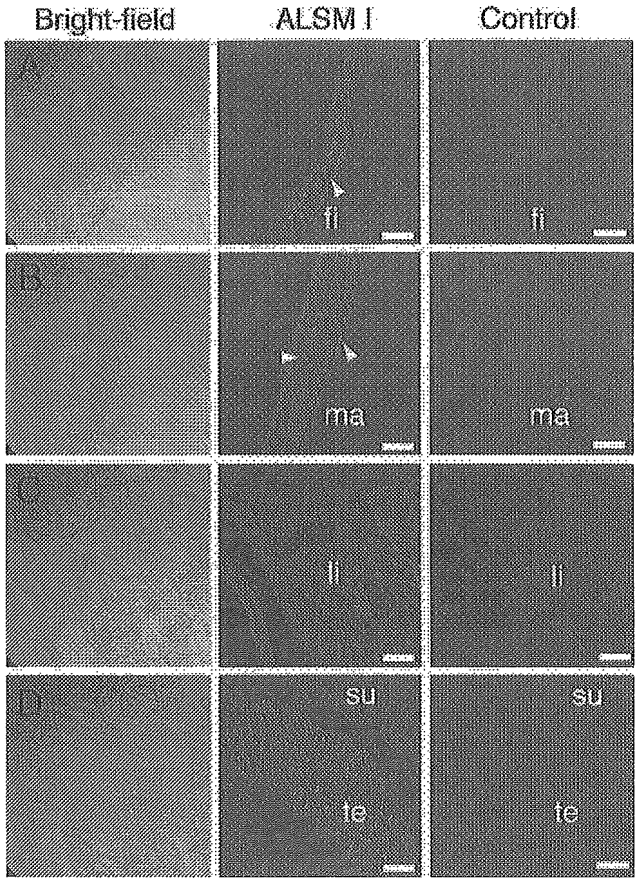

Fig. 4. Higher-magnification images of the tissue distribution of ALSM I. Merged images shows the distribution of cellular actin (red) and ALSM isoforms (green). Immunofluorescence analysis detected ALSM I staining in muscle tissues, including (A) lateral fin (fi), (B) mantle (ma), and (D) tentacle (te). Strong staining was also detected in (C) the liver (li). (Control), Negative control in the absence of primary antibody. su, sucker. Bars indicate 50 μm.

2B, right panel). Immunoblot analysis of tissue extracts showed a doublet at stage 28 (10 weeks), with a major 45-kDa band and a minor 50-kDa band (Fig. 2C). Thus, we concluded that the antibodies specifically recognized each isoform.

3.2. Tissue distributions of ALSM isoforms in embryos

We examined the embryonic tissue distribution of ALSM isoforms by indirect immunofluorescence analysis. ALSM is a secreted protein reportedly localized in the extracellular region of the mantle muscle (Yokozawa et al., 2002). Distribution in other tissues has not been reported. To determine the extracellular localization, we performed double immunostaining with the ALSM antibodies and an actin antibody, which recognizes cytoplasmic actin (Fig. 3). With both ALSM antibodies, a strong green signal was identified in the retina. However, a similar signal was seen in the absence of primary antibody as described below, suggesting that the signal in the retina was due to autofluorescence. Staining for ALSM I was detected in muscle tissues, including mantle, fin, and tentacles. In contrast, no obvious staining for ALSM III was detected in muscle tissues except fin. Both ALSM I and III staining was detected in the fin. ALSM I staining was distributed over the fin (Fig. 4a), whereas ALSM III staining in the fin was confined to the central area (Fig. 5a). Staining for ALSM I and III was detected in the liver (Figs. 4c and 5c) and the membranous tissue surrounding the inner yolk (Fig. 5b). Interestingly, staining for ALSM IIII was obvious in the iris (Fig. 5e) and in tissue connected to the cornea (Fig. 5d). However, no staining for ALSM I was detected in these regions.

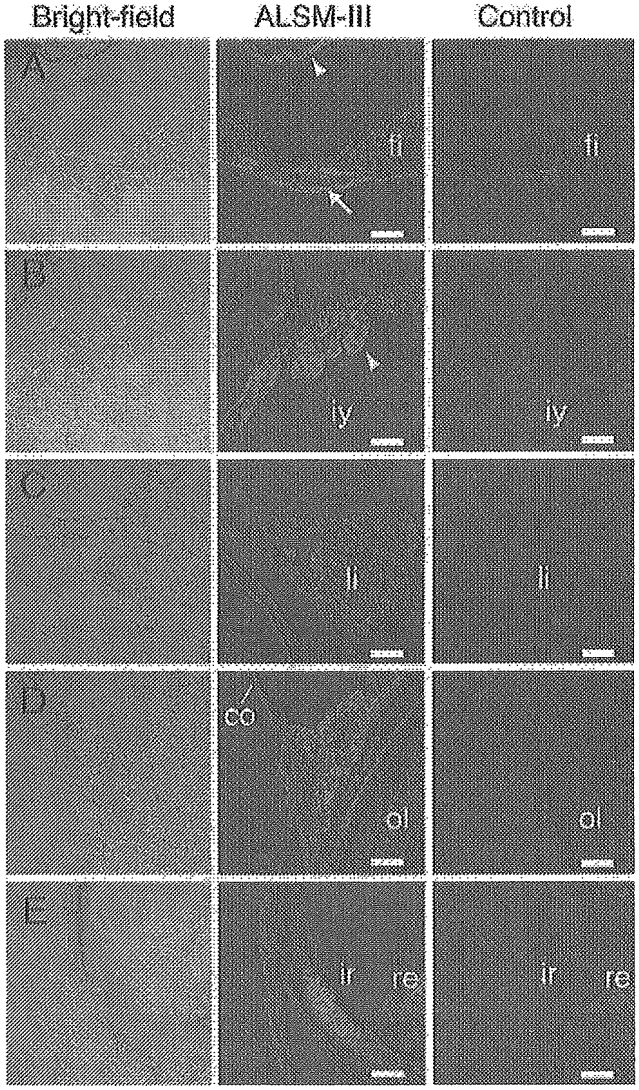

Fig. 5. Higher-magnification images of tissue distribution of ALSM III. Merged images shows the distribution of cellular actin (red) and ALSM isoforms (green). Immunofluorescence analysis detected ALSM III in (A) center area of the fin (fi) as indicated by arrow and in membranous tissue surrounding the inner yolk (iy) as indicated by arrowheads in (A) and (B). Strong staining was detected in (C) the liver (li) compared to the negative control in the absence of primary antibody. ALSM III staining was also detected in (D) tissue connected to the cornea (co) and in (E) the iris (ir). ol, optic lobe. (re) represents the non-specific autofluorescence detected in retina. Bars indicate 50 μm.

We reported that immunoblot analysis showed ALSM I to be distributed in a wide variety of tissues in adult spear squid (Yokozawa et al., 2002). However, expression of ALSM mRNA has not been reported. In situ hybridization analysis of stage 28 embryos showed expression of ALSM I mRNA to be confined to the liver (Fig. 6B and D). However nonspecific sense signals were present in the lower tip of the body and in the ink sac, retina, and cornea (Fig. 6A). In the optic lobe, signals detected with the anti-sense probe were stronger than those detected with the sense probe. However, this may also have been nonspecific background. Nonspecific signals were also detected at the lower tip of the body and in the retina in stage 26 embryos, and no obvious differences were identified between sense and anti-sense probes at this stage (Fig. 6E and F).

3.3. Tissue distributions and expression of ALSM isoforms in adult squid

To examine the expression levels of ALSM isoforms in adult squid, specific probes for northern blot analysis were prepared by PCR amplification. Probes for ALSM I and III were 68% and 58% identical to the corresponding sequences of each isoform. Probe specificity was further confirmed by Southern blot analysis against isolated cDNA clones (data not shown). With northern blotting, each isoform was detected below the ribosomal RNA (approximately 2 kb), and the staining was detected only for the liver (Fig 7A). Consistent with biochemical findings (Tamori et al., 1999; Yokozawa et al., 2002), signals for ALSM III were stronger than signals for ALSM I. Restricted expression was further analyzed by RT-PCR (Fig. 7B). Approximately 30 ng of complementary DNAs for each isoform was used as template. Actin as an internal control was detected in all tissues. Amplified fragments for each isoform were detected only in the liver. Thus, expression of ALSM isoforms seems to be restricted to the liver of adult squid.

We reported previously that ALSM I was widely distributed in tissues (Yokozawa et al., 2002). In this study, we examined tissue distribution of ALSM III. An immunoreactive band was detected at 45 kDa; staining was prominent for digestive organs, including stomach, liver, and pancreas and week in muscle tissues such as branchial heart, mantle, and tentacle (Fig. 8); a 30-kDa degradation product of ALSM was mainly detected in the mantle. In embryos, staining of ALSM III was present in the iris and in tissue connected to the cornea. However, no immunoreactive bands were detected by immunoblotting of adult squid eyes. Distribution of ALSM III was further examined by double immunostaining with anti-actin antibody. Patchily staining of ALSM III was detected (Fig 9B) and distributed extracellularly in the mantle muscle (Fig. 9C), unlike the intracellular distribution of actin (Fig. 9A). Squid liver consists of hepatic lobules, as indicated by the dashed-line in Fig. 9D. Staining of actin was detected in the boundary area of the lobules (double arrowhead in Fig. 9E) and periphery of the central vein (arrowheads in Fig. 9E). Strong staining of ALSM III was detected in hepatic cells, and

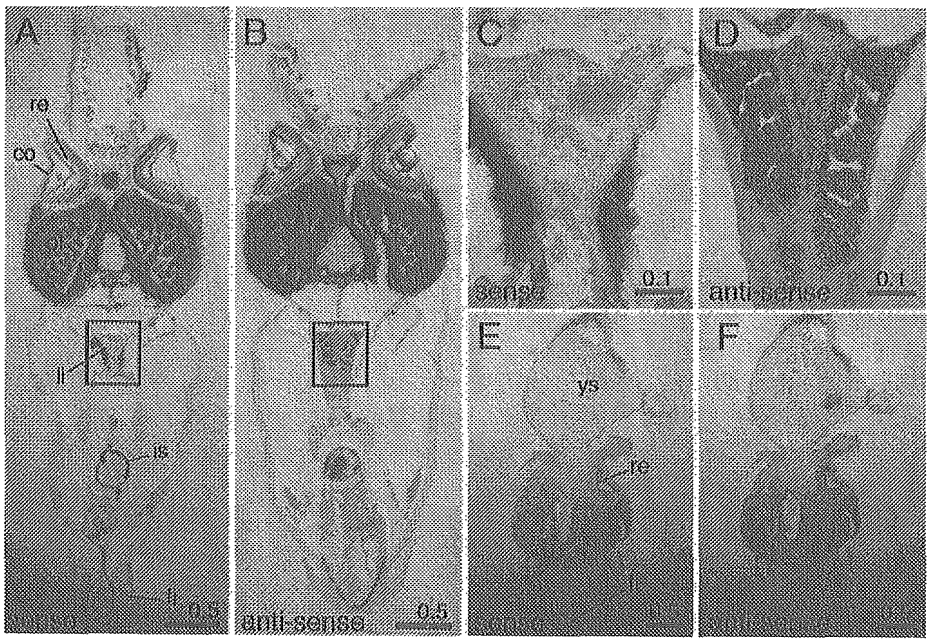

Fig. 6. In situ hybridization. Sections (16-μm thickness) were prepared from frozen squid embryos at stage 28 (A, B, C, and D) and 26 (E and F). Sense and anti-sense riboprobes were used to detect specific signal for ALSM I mRNA. (C and D), High-power views of boxed areas in A and B show expression of ALSM I mRNA in the liver (li). Non-specific sense signals were seen in lower tip of body near the fin (fi), ink sac (is), retina (re), and cornea (co) at stage 28 embryo. Bars in A, B, E, and F are 0.5 mm; bars in C and D are 0.1 mm. ys, yolk sac.

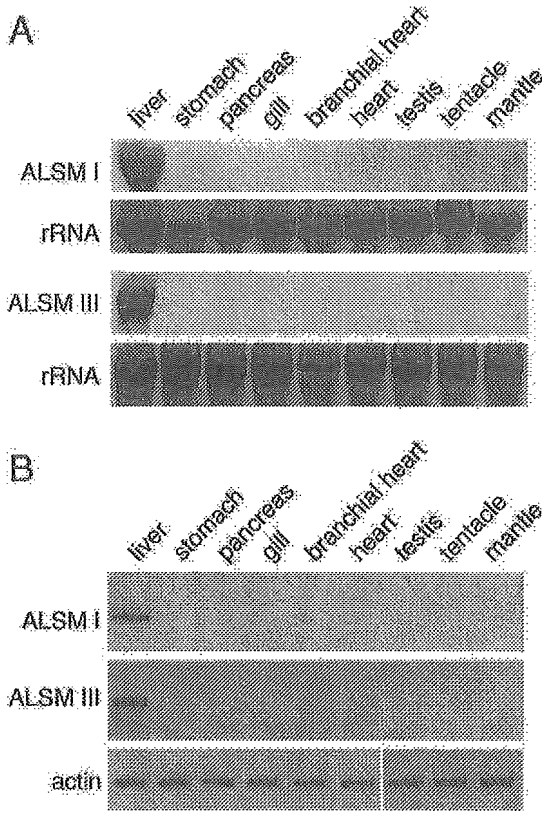

Fig. 7. mRNA expression of ALSMs in adult squid. (A) Northern blot analysis of ALSM isoforms in tissues of adult spear squid. Approximately 30 μg of total RNA was separated on 1% agarose/formaldehyde gels, stained with ethidium bromide (lower panes), and hybridized with specific probes (ALSM I and ALSMIII in upper panes). rRNA, ribosomal RNA. (B) RT-PCR analysis of ALSM isoforms in tissues of adult spear squid. Complementary DNAs (cDNAs) were reverse-transcribed from total RNAs with oligo-dT primer. Approximately 30 ng of cDNA was used as template in the PCR reaction under the conditions described in the Materials and methods.

weak staining was detected in interlobular artery or interlobular vein (Fig. 9F).

4. Discussion

Astacins are widely distributed in vertebrates and invertebrates. Recent analysis has shown that astacins are associated with a wide range of physiologic events and that some astacins are multifunctional proteases (Bond and Beynon, 1995; Sarras, 1996). The genome-sequencing of *Caenorhabditis elegans* identified 40 genes that code for astacin-like proteins, and they are classified into six groups by comparison of the highly conserved protease domain and unique C-terminal domain. Their expression levels and profiles are highly organized developmentally (Mohrlen et al., 2003). One astacin group with conserved protease and MAM domains has been identified in squid. Two isoforms, ALSM I and II for Japanese common squid and ALSM I and III for spear squid have been cloned and characterized. ALSM was originally identified as a metalloprotease, which hydrolyzes MyHC specifically, and was thought to be involved in muscle metabolism (Okamoto et al., 1993). However, our recent analysis has shown that ALSM is a secreted protease. To elucidate the physiologic roles of ALSM in vivo, we examined embryonic expression and distribution of ALSM isoforms. Tracking squid throughout their lives can be difficult, and handling and feeding techniques for spear squid are not well established. Survival after hatching in small aquariums is quite low (Y. Ikeda, personal communication). In the present study, we obtained squid embryos at three stages of development. To determine ALSM tissue distributions, we used specific antibodies for ALSM I (TY-ID, (Yokozawa et al., 2002)) and III (KY-III). These antibodies are specific to each isoform, as shown in Fig. 2. However, bands detected in extracts from stage 28 embryos were seen as doublets, indicating that the antibodies recognize not only the mature protein (45 kDa) but also the precursor peptide (50 kDa) of each isoform. With the same antibodies, only a single band (45 kDa) was detected in tissue extracts from adult spear squid (Fig. 8B), suggesting the presence of a mechanism controlling the differentiation of precursor ALSM to mature ALSM. The physiological roles of astacins in development have been well studied in fish. HCE and LCE of medaka are choriolytic enzymes secreted from unicellular hatching glands to digest the egg envelope. Expression of HCE and LCE is detected in the late gastrula until just before hatching (Inohaya et al., 1995; Hiroi et al., 2004). Immunoblot analysis revealed that ALSM isoforms are expressed in

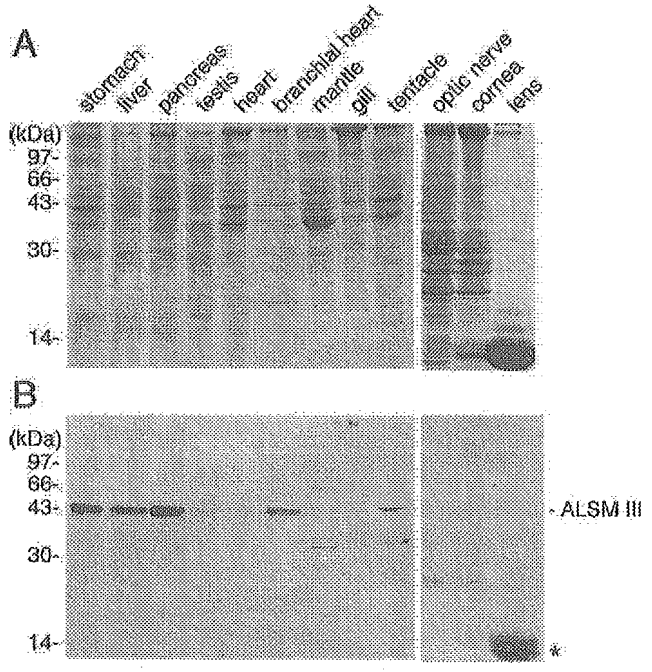

Fig. 8. Tissue distribution of ALSM III in adult spear squid. Proteins from various tissue extracts (15 μg) were electrophoresed on SDS-polyacrylamide gels (A) and subjected to immunoblotting with an affinity purified polyclonal antibody, KY-III (B). Asterisk indicates non-specific staining of lens crystallin.

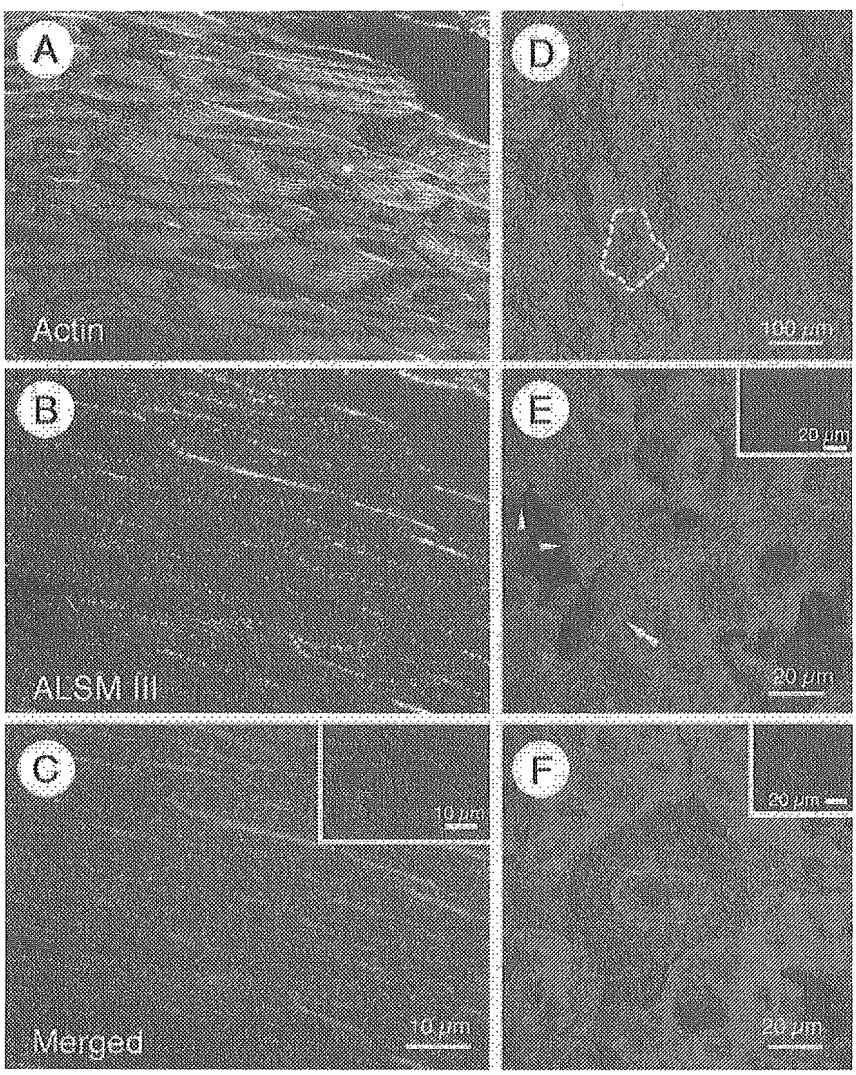

Fig. 9. Immunohistochemical distribution of ALSM III in adult spear squid. Sections of the mantle muscle (A–C) and the liver (D–F) were double stained with anti-actin antibody (red) and KY-III (green). Staining of ALSM III was patchy (B) and distributed extracellularly, unlike the intracellular distribution of actin (A). C, Merged image of (A) and (B). D, Macroscopic view of the liver section with double immunostaining. Squid liver consists of hepatic lobules (dashed-line), like mammal liver. E, High magnification view of boundary area of hepatic lobules. Staining of actin was detected in the boundary area of hepatic lobules (double arrowhead) and periphery of the central vein (arrowheads), whereas staining of ALSM III was detected in hepatic cells. F, High magnification view of interlobular vein. A few layers of actin staining were observed in the vein, whereas staining of ALSM III was weaker in the vein than in hepatic cells. Insert in panel C, E and F shows negative control in the absence of KY-III.

newly hatched squid embryos (stage 28). No immunoreactivity was identified in early stage embryos, which is consistent with in situ hybridization (Fig. 6E and F) and indirect immunofluorescence data (data not shown). Thus, expression of ALSM in squid is unlike that of hatching enzymes. Embryonic expression of astacin family proteins has also been reported in hydra (*Hydra vulgaris*). HMP-1 is secreted from body column endodermal cells at the apical pole, where head regeneration occurs, and it translocates to the tentacles. HMP-1 is involved in cell differentiation or transdifferentiation in tentacle and head regeneration (Yan et al., 1995, 2000b). Both ALSM isoforms were distributed in the fin of the squid embryo; however, ALSM III was confined to the apical region of the fin, suggesting that at least one ALSM isoform contributes to developmental events, as is the case for HMP-1. Distribution of ALSM III in mantle muscle also seems to be developmentally regulated because no detectable immunofluorescence signals were observed in embryonic mantle muscle, whereas apparent singles were detected extracellularly, which is similar to that of ALSM I (Yokozawa et al., 2002).

As shown in Fig. 6, expression of ALSM I mRNA was observed in the liver, and no signal was identified in other tissues. Expression of ALSM III mRNA was also restricted to the liver of embryos (data not shown). Northern blotting and RT-PCR analysis revealed that expression of ALSM mRNAs was restricted to the liver even in the adult squids, suggesting ALSMs are provided only from the liver, beginning at the later stage of embryogenesis and continuing to maturity. However, immunofluorescence study and